

## ABSTRACT

Title of thesis: MANUFACTURABILITY ANALYSIS OF  
THERMALLY-ENHANCED  
POLYMER COMPOSITE HEAT EXCHANGERS

Timothy Ryan Hall, Master of Science, 2011

Thesis directed by: Professor Satyandra K. Gupta  
Department of Mechanical Engineering,  
Institute for Systems Research

Thermally-enhanced polymer composite heat exchangers are an attractive alternative for applications such as the use of seawater as a cooling medium and other corrosive environments that traditionally use expensive exotic metallic alloys, but a number of manufacturing challenges exist. The goal of this thesis is to develop an understanding of the manufacturing feasibility, in particular mold filling and fiber orientation, of utilizing thermally-enhanced polymer composites and injection molding to manufacture polymer heat exchangers.

To best predict mold filling feasibility, this thesis proposes developing an explicit construction of the boundary, represented as a surface based on the parameter space, which separates the feasible and infeasible design space. The feasibility boundary for injection molding in terms of the design parameters is quite complex due to the highly nonlinear process physics, which, consequently, makes molding simulation computationally intensive and time consuming. This thesis presents a new approach for the explicit construction of a moldability-based feasibility bound-

ary based on intelligent Design of Experiments and adaptive control techniques to minimize the number or computation experiments needed to build an accurate model of the feasibility boundary. Additionally, to improve the flexibility of the mold filling prediction framework to changes in overall heat exchanger design, a model simplification approach is presented to predict mold filling for general finned-plate designs by determining an equivalent flat plate representation and utilizing a developed flat plate mold filling metamodel to estimate mold filling. Finally, a fiber orientation measurement methodology is presented for experimentally determining fiber orientation behavior for sample heat exchanger geometries that develops both a local and global understanding of the fiber orientation behavior and compares thesis findings to simulation predictions.

The work presented in this thesis significantly advances the understanding of manufacturability considerations for utilizing thermally-enhanced polymer composites in heat exchanger applications and is useful in design exploration, optimization, and decision-making approaches.

MANUFACTURABILITY ANALYSIS OF  
THERMALLY-ENHANCED  
POLYMER COMPOSITE HEAT EXCHANGERS

by

Timothy Ryan Hall

Thesis submitted to the Faculty of the Graduate School of the  
University of Maryland, College Park in partial fulfillment  
of the requirements for the degree of  
Master of Science  
2011

Advisory Committee:  
Professor Satyandra K. Gupta, Chair/Advisor  
Professor Hugh A. Bruck  
Professor Avram Bar-Cohen

© Copyright by  
Timothy Ryan Hall  
2011

## Acknowledgments

First and foremost, I would like to express my sincere gratitude and appreciation to Dr. Gupta for being an excellent advisor. His mentoring and guidance was critical to completing this research and, more importantly, helped me grow and develop into a better student, engineer, and person. His vision and focus for the many facets of my research were invaluable in guiding me to discover new and exciting avenues to explore. I would like to thank Dr. Bruck for his patience and guidance during the development of my thesis and his keen perspective on the challenges that I encountered. I would also like to acknowledge Professor Bar-Cohen for serving on my thesis committee and providing valuable insight and advice as I have progressed through this experience.

I would like to express my thanks to the PHX group that I was fortunate to be a part of. We spent many hours together working through new ideas and trouble-shooting problems and my work is more balanced and rich because of it. Also, I would like to express my appreciation for Dr. Gupta's research group and the amazing people that it has introduced me to. Countless days and nights in the lab have led to wonderful relationships and exposure to such a range of personalities has kept every day rewarding and exciting.

I owe special thanks to Madan and Vaishnavi for their invaluable assistance in developing this work. Madan kept pushing me to broaden my understanding of the world surrounding my research and together we searched new frontiers. Without Vaishnavi I couldn't have found a single fiber and her work helped me achieve new

possibilities. I would also like to thank Wojciech, Leicester, Juan, Frank, and Bill for all of their help and encouragement along the way.

This research was performed as part of the Energy Education and Research Collaboration (EERC) between the University of Maryland and The Petroleum Institute and I would like to thank the Abu Dhabi National Oil Company (ADNOC) and its international partners for their generous financial support and the opportunity to explore such new and exciting work.

Most importantly, I want to thank my family and my wife, Jennifer. You are the most important people in my life and I will always love you. Your support has been unwavering since I began this journey and I could not have done this without you. Jennifer, Mom, Dad, and all of my family, this work is dedicated to you.

# Table of Contents

List of Figures	vi
List of Abbreviations	viii
1 Introduction	1
1.1 Background . . . . .	1
1.1.1 Polymer Heat Exchangers . . . . .	1
1.1.2 Injection Molding . . . . .	2
1.1.3 Polymer Composites . . . . .	4
1.2 Motivation and Challenges . . . . .	5
1.3 Thesis Goals and Scope . . . . .	7
1.4 Organization . . . . .	9
2 Explicit Construction of Moldability-based Feasibility Boundary	11
2.1 Introduction . . . . .	11
2.2 Background . . . . .	12
2.3 Related Work . . . . .	13
2.3.1 Application of Metamodeling Techniques . . . . .	13
2.3.2 Classification Methods . . . . .	15
2.4 Problem Definition . . . . .	15
2.5 Approach . . . . .	17
2.5.1 Feasibility Boundary Search Algorithm . . . . .	17
2.5.2 Transition Point Search Algorithm . . . . .	22
2.5.3 Problem Formulation Details . . . . .	24
2.6 Results and Discussion . . . . .	29
2.6.1 Transition Region Identification . . . . .	30
2.6.2 Assessment of Prediction Performance . . . . .	31
2.7 Summary . . . . .	34
3 Feature Removal for Efficient Assessment of Mold-Filling Feasibility of Finned-Plate Geometries	37
3.1 Introduction . . . . .	37
3.2 Background . . . . .	38
3.3 Related Work . . . . .	38
3.4 Problem Definition . . . . .	41
3.5 Approach . . . . .	42
3.5.1 General Flat Plate Mold Filling Metamodel . . . . .	42
3.5.2 Localized Flat Plate Mold Filling Metamodel . . . . .	47
3.5.3 Model Simplification - Disc-Fin Model . . . . .	49
3.6 Results and Discussion . . . . .	54
3.7 Summary . . . . .	58

4	Development of a Fiber Orientation Measurement Methodology	60
4.1	Introduction	60
4.2	Background	61
4.3	Related Work	63
4.3.1	Fiber Orientation	63
4.3.2	Experimental Methodologies	66
4.4	Problem Definition	68
4.5	Approach	69
4.5.1	Experimental Setup	69
4.5.2	Fiber Orientation Comparison Framework	71
4.5.3	Image Processing Algorithm	73
4.5.4	Tensor Calculation	76
4.5.5	Comparing Experimental and Simulation Results	77
4.5.6	Problem Formulation Details	80
4.6	Results and Discussion	82
4.7	Summary	91
5	Conclusion	94
5.1	Intellectual Contributions	94
5.2	Anticipated Benefits	95
5.3	Future Work	96
5.3.1	Improvement to Feasibility Boundary Search Algorithm	96
5.3.2	Advancements in Model Simplification Approach	97
5.3.3	Refinements for Fiber Orientation Measurement Methodology	98
	Bibliography	99

## List of Figures

1.1	Babyplast injection molding machine. . . . .	3
1.2	Process profile for injection molding. . . . .	3
2.1	Comparison between classification methods and proposed method, noting implicitly vs explicitly discovered feasibility boundary and adaptive Design of Experiments. . . . .	16
2.2	Flow diagram for the Feasibility Boundary Search Algorithm for predicting the location of the transition boundary for a candidate design. . . . .	18
2.3	Overview of Feasibility Boundary Search Algorithm. . . . .	19
2.4	Transition Point Search Algorithm. . . . .	22
2.5	Plate fin design. . . . .	24
2.6	Selective search behaviors. . . . .	28
3.1	Example medial axis transform of shape whose boundary is the outer closed curve. [4] . . . . .	41
3.2	Flat plate mold filling metamodel trends. . . . .	44
3.3	Flat plate mold filling metamodel trends, continued. . . . .	45
3.4	Localized flat plate mold filling metamodel. . . . .	49
3.5	Disc-fin geometry. . . . .	50
3.6	Model simplification details. . . . .	52
3.7	Scaled thickness flat plate simplification results with no tuning factor. . . . .	53
3.8	Application of tuning factors, including an ideal tuning factor. . . . .	54
3.9	Example of randomly-generated finned-plate design. . . . .	55
3.10	Model simplification results. . . . .	56
4.1	The effect of processing parameters on part performance due to fiber orientation. . . . .	60
4.2	Stress-strain curve for varying fiber orientation and loading of a sample geometry. [21] . . . . .	62
4.3	Vector representing fiber orientation. . . . .	64
4.4	Example tensor values. . . . .	64
4.5	Fiber cross-section for determining orientation. . . . .	65
4.6	Issue resolving sign of out-of-plane angle using simple cross-section. . . . .	65
4.7	Progression of image processing algorithm for identifying fibers, described in Section 4.5.3. . . . .	74
4.8	Elliptical fiber cross-section for determining orientation. . . . .	77
4.9	L-Channel mold with parts. . . . .	80
4.10	Sectioning plane for test geometry. . . . .	82
4.11	L-Channel polishing jig. . . . .	82
4.12	Example of collected microscope image with image processing results overlaid on lower half. . . . .	84
4.13	Measurement validation image. . . . .	84
4.14	Moldflow <sup>®</sup> tensor component results. . . . .	87

4.15 Tensor results. . . . .	89
4.16 Detailed tensor results. . . . .	90

## List of Abbreviations

$a_{ij}, t_{ij}$	Fiber Orientation Tensor Component
$f$	Response Value
$F$	Fin Height
$H$	Base Thickness
$k$	Tuning Variable
$k_p$	Proportional Control Variable
$L$	Base Length
$m$	Minor Axis Length
$M$	Major Axis Length
$p$	Fiber Vector
$P$	Injection Pressure
$Q$	Injection Flow Rate
$r$	Injection Filled Radius
$S$	Fin Spacing
$T$	Injection Melt Temperature
$V$	Volume
$W$	Fin Width
$z$	Search Dimension
AML	Advanced Manufacturing Lab
CAD	Computer-Aided Design
CAE	Computer-Aided Engineering
DoE	Design of Experiments
FEA	Finite Element Analysis
PHX	Polymer Heat Exchanger
SEM	Scanning Electron Microscope
SVM	Support Vector Machine
V/P	Velocity / Pressure Switchover Point

# Chapter 1

## Introduction

### 1.1 Background

#### 1.1.1 Polymer Heat Exchangers

The utilization of polymers in heat exchangers is attractive due to their relatively low cost and weight, lower fabrication energy and lifecycle energy usage than equivalent metal heat exchangers [53], and corrosion and fouling resistance [71]. DuPont developed the first polymer heat exchanger in 1965 using flexible Teflon<sup>®</sup> tubing in a shell-and-tube configuration [59]. The introduction of new thermally-enhanced polymer composites and manufacturing processes has led to renewed interest in polymer heat exchangers and emerging applications previously supported only by heat exchangers made of exotic metallic alloys. Industrial applications which utilize seawater as a cooling medium for heat exchangers traditionally require exotic alloys to survive the corrosive environment, leading to dramatically increased costs and processing requirements. Polymer composites utilizing thermally-enhanced fillers, such as pitch-based carbon fiber, have led to orders of magnitude improvement in overall thermal conductivity, making them competitive with corrosion-resistant metals such as titanium and copper-nickel alloys. [7]

This study is primarily interested in large, plate-type heat exchanger geome-

tries and the majority of the findings will be useful for any application using similar plate-type geometries. Two of the most promising advances in polymer heat exchangers are the use of injection molding for manufacturing and the application of advanced thermally-enhanced polymer composites. An overview of these are shown in the following sections and are described in more detail in the relevant technical chapters.

### 1.1.2 Injection Molding

Injection molding is one of the most popular methods for manufacturing polymer components and is used to produce a wide range of products with varying shapes and sizes [10, 9, 32, 55, 58]. In this process, the polymer is heated over its melting point and then injected into a mold cavity under high pressure. This melt then solidifies, taking the shape of the cavity and forming the part. After the melt has solidified, the mold opens, the part is ejected from the mold, the mold closes and the process is repeated. After a mold has been manufactured, a high volume of molded components can be produced quickly and inexpensively. The injection molding machine used in the Advanced Manufacturing Laboratory (AML) at the University of Maryland is shown in Figure 1.1.

The injection molding process consists of three stages, detailed in Figure 1.2. First, the injection molding machine forces liquefied polymer into the mold cavity at a constant flow rate, adjusting injection pressure and other parameters to achieve this. When the maximum injection pressure is reached, known as the velocity /



Figure 1.1: Babyplast injection molding machine.

pressure switchover point (V/P), the polymer is forced into the mold cavity at a constant pressure in order to protect machine equipment. Finally, after the part has solidified and no more material can be forced into the mold, a constant packing pressure is applied for a set time interval to alleviate shrinkage and other undesirable behavior that can occur as the part cools.

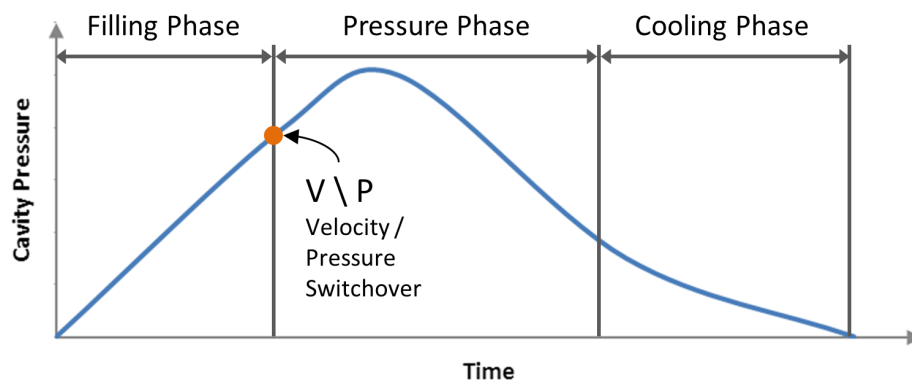


Figure 1.2: Process profile for injection molding.

In general, there are three components that affect injection molding performance: injection molding processing parameters, material properties, and mold

design. Processing parameters primarily consist of the maximum injection pressure, the injection flow rate, and the mold temperature. Material properties include the melting temperature and viscosity of the polymer. Mold design factors include the injection location, runner design, mold material, cooling channel design, and the design of the component to be molded.

### 1.1.3 Polymer Composites

Using injection-moldable, filled polymer composites has gained popularity over the last decade for enhancing the functionality of produced components [5, 6, 11, 12, 13, 23, 26, 27, 40, 39]. Using traditional polymer matrices, such as Nylon, fillers ranging from clay particles to carbon fibers are introduced, leading to potentially dramatic changes in the overall material properties of the composite.

Of particular interest to this project is the introduction of carbon fiber fillers at high concentrations leading to significant improvement in the thermal conductivity of the resulting thermally-enhanced polymer composite [7]. These materials have manufacturing challenges due to their high thermal conductivity and high filler concentration. Increased thermal conductivity leads to the polymer melt losing heat quickly during the injection molding process and potentially solidifying before the mold has completely filled, known as a short shot. Additionally, the high filler concentration increases the viscosity of the polymer material, making the injection molding process more difficult due to parameters such as reaching the V/P too quickly and potentially leading to a short shot. Additionally, the orientation of

fibers embedded in polymer composites can lead to directionality or anisotropy in the produced material properties and can therefore affect the overall component performance. These manufacturing challenges must be fully understood to properly design components for injection molding with thermally-enhanced polymer composites.

## 1.2 Motivation and Challenges

The high thermal conductivity of thermally-enhanced polymer composites and the ability to be injection molded makes them extremely attractive for applications such as polymer heat exchangers but present challenges for manufacturing which must be addressed. Therefore, developing an understanding of the manufacturability of thermally-enhanced polymer composites in heat exchanger applications is of critical importance for successfully designing thermally-enhanced polymer heat exchangers.

As injection molding has gained popularity over the past decades, a thorough understanding of the process has been developed. This understanding includes a wide set of design guidelines for properly designing components for injection molding and process estimates for predicting the suitability of injection molding for seemingly any geometry. Unfortunately, the advanced and unusual material properties of thermally-enhanced composites restricts the use of this knowledge base and necessitates the use of intensive tools for predicting injection molding performance. These tools are not suitable for applications which require rapid iterations and the

evaluation of many designs, such as design exploration or optimization.

The complex behavior inherent in injection molding and the addition of advanced thermally-enhanced materials prevents the use of traditional physical modeling techniques and therefore requires Computer-Aided Engineering (CAE) methods such as Finite Element Analysis (FEA) to predict injection molding performance. These methods require intricate finite element meshes and elaborate governing equations that make the process computationally-expensive and resource intensive. Moldflow, the industry standard injection molding simulation tool, can take up to 4 hours to mesh and simulate a candidate heat exchanger geometry.

The overarching goal of the polymer heat exchanger design project is to develop an optimization framework for designing thermally-enhanced polymer heat exchangers that takes into account thermal, structural, and manufacturing considerations and finds the optimal heat exchanger design for the given design criteria. Due to the nature of optimization applications, a multitude of heat exchanger designs will be evaluated to determine the manufacturing feasibility and therefore the manufacturability component of the framework must be sufficiently computationally efficient.

In addition to determining the manufacturing feasibility of a candidate heat exchanger geometry, understanding the fiber orientation behavior is an important aspect of developing an understanding of the manufacturability of thermally-enhanced polymer heat exchangers. Due to the inherent geometry of the introduced fibers, the thermal and structural improvements are primarily along the length of the fiber and are relatively minimal in the transverse direction. This leads to an anisotropic mate-

rial property distribution within manufactured components that is tied to the fiber orientation behavior within the part. Manufacturing parameters and part design play a key role in determining fiber orientation and therefore component performance and it is therefore of utmost importance to understand how manufacturing considerations affect fiber orientation.

Advanced fiber orientation models have been developed in conjunction with the progress in developing fiber-filled polymer composites and have been integrated into injection molding simulation tools such as Moldflow. Unfortunately, the effect of thermally conductive fibers has not been sufficiently studied and is not taken into account in the currently applied fiber orientation models. It is therefore important to develop an understanding of the actual fiber orientation behavior of thermally-enhanced composites in experimental samples and determine the applicability of the current fiber orientation models and cases in which they may be insufficient.

### 1.3 Thesis Goals and Scope

The goals and scope of this thesis revolve around developing an understanding of the manufacturability of thermally-enhanced polymer composites for polymer heat exchanger applications with the intent of implementing the findings in a design optimization framework. This is divided into two primary goals: developing a computationally-fast framework for predicting injection molding feasibility and creating an experimental methodology for determining fiber orientation in polymer heat exchanger sample geometries.

Due to the computationally-expensive nature of injection molding simulation, a model must be developed for predicting mold filling, an important measurement of the feasibility of injection molding, for thermally-enhanced polymer heat exchangers for use in design exploration or optimization applications. This model should provide an accurate estimate of the mold filling for a candidate heat exchanger geometry, give useful response information for improving subsequent designs, and be computationally fast, dramatically reducing prediction time compared to traditional injection molding simulation. Additionally, this model should be flexible to changes in the overall heat exchanger geometry in order to be applicable to alternative designs.

In order to completely understand the fiber orientation behavior for a given polymer heat exchanger design, an experimental methodology should be developed for efficiently measuring fiber orientation in sample geometries. This methodology will involve sectioning and polishing samples for imaging, collecting microscope images of the area of interest, performing image processing to extract fiber information from the collected images, and applying fiber orientation calculation techniques to determine the fiber orientation information for the sample section. This information will be compared to simulation predictions to analyze the effectiveness of currently implemented fiber orientation models and outline cases where such models may be unsuitable. The developed model should be flexible to a range of potential heat exchanger geometries, should be applicable over large test regions to develop a more global understanding of the fiber orientation behavior in a test sample, should provide control over the quality of the collected fiber orientation information, and

should provide both a quantitative and qualitative insight into the fiber orientation within the sample and how it compares to simulation predictions.

## 1.4 Organization

**Chapter 2** presents the development of a computationally-fast, accurate feasibility boundary for predicting the mold filling performance of plate-fin polymer heat exchanger design. In developing this model, a new approach, entitled feasibility boundary search, is presented which uses advanced Design of Experiments and adaptive control techniques to create a highly accurate feasibility boundary over a wide design range while using minimal computationally-expensive simulations. The feasibility boundary is useful for both determining the manufacturing feasibility of a candidate plate-fin heat exchanger design as well as predicting the minimum achievable plate thickness for optimizing the heat transfer properties of the developed heat exchanger.

**Chapter 3** presents a model simplification framework for predicting mold filling in general plate-protrusion designs. This approach allows greater flexibility in the general heat exchanger design and is useful for evaluating the manufacturability of new heat exchanger design concepts. The model simplification framework is used to calculate an equivalent flat plate representation of the finned plate geometry and then applying a simple flat plate mold filling metamodel to predict mold filling.

**Chapter 4** presents a fiber orientation measurement methodology for collecting experimental samples, performing microscope imaging and extracting fiber

orientation information for comparison with simulation predictions and for understanding when predictions may not be suitable and measured behavior should be utilized instead. The developed method aimed to satisfy the following goals: use low magnification imaging to collect fiber orientation images, utilize a single section when preparing samples, employ the goal material for experimental samples, control the fiber orientation measurement region, and use standardized tools for image processing and fiber orientation calculation techniques. In fulfilling these goals, the developed fiber orientation measurement methodology is useful in a wide variety of fiber orientation measurement applications while maintaining sufficient accuracy and effectiveness.

## Chapter 2

### Explicit Construction of Moldability-based Feasibility Boundary

#### 2.1 Introduction

Injection molding is one of the most widely used manufacturing methods for polymer components and its rapid cycle times and ability to create complex geometries makes it an attractive solution for many applications. The complex physical behavior of injection molding has led to the use of methods such as finite element analysis and other computer-aided engineering (CAE) techniques in order to analyze mold filling [56], an essential feasibility consideration when evaluating a potential component design. Additionally, since in many design situations it is highly likely that the optimal solution will be found at the boundary defining feasibility and therefore it is useful to know both the feasibility of a proposed design and the feasibility boundary. Incorporating manufacturing feasibility is a very important consideration during the design and optimization processes and the complex nonlinear physics that govern many manufacturing processes require computer simulation to determine manufacturing feasibility. While such simulation has proven invaluable to the field of injection molding and other manufacturing applications, it is computationally expensive and therefore not suitable for design exploration and optimization situations.

As computer analysis techniques have become more complicated, it has become

useful to devise approximations of the underlying model, a 'model of the model' or *metamodel*, to improve the efficiency of performing advanced analyses [43]. The application of metamodeling techniques, which predict response values based on a set of design experiments [75], has been successful in applications ranging from the optimization of the air flow rate in aircraft jet engines, in which [33] described experiments requiring a day to two weeks to complete, to crash simulation, which Ford Motor Company reports takes 36-160 hours per simulation [57]. Metamodeling is an integral component in these and other computationally-expensive applications and this study proposes a method of developing a metamodel for predicting the moldability of polymer heat exchangers.

## 2.2 Background

One of the primary concerns when designing products for injection molding is moldability, whether the use of injection molding is feasible for a given design, primarily from the point of view of mold filling. Moldability is especially important for potential polymer heat exchanger applications which have very large components and relatively expensive materials for which a failure to fill could have dramatic cost effects. Additionally, the unusual properties of the thermally-enhanced polymers utilized, including high viscosity and thermal conductivity, combined with the large scale and thin wall thickness of the investigated heat exchanger designs introduce further complexity into the mold filling process. Finally, since conductive heat transfer increases as thickness decreases [37], the optimal heat exchanger design

often occurs at the minimum thickness that is feasible for mold filling and therefore it is very useful for the designer to know the location of the feasibility boundary.

Based on the requirements described above, there are two primary design criteria that should be considered when analyzing the moldability of a polymer heat exchanger and in general applications where constrained optimization is utilized:

1. Is the design feasible?
2. Where is the feasibility boundary located, explicitly?

As discussed previously, CAE techniques such as finite element analysis are commonly applied to analyze mold filling in injection molding [56], but they are computationally expensive and consequently the development of a method for predicting moldability is beneficial for applications which require numerous simulations, such as optimization.

## 2.3 Related Work

### 2.3.1 Application of Metamodeling Techniques

The development of a computationally-fast metamodel is an apt approach for approximating moldability, although the goal of both predicting feasibility and accurately estimating the feasibility boundary may be challenging. Traditional statistical metamodeling involves collecting a range of experiments across the design space and then applying a model to the discovered response values to approximate the response space.

Traditionally, standard Design of Experiments (DoE) methods have been applied to ensure that the developed model is useful across the entire design space. Methods include fractional or factorial DoE, Central Composite Designs, or space filling methods such as Latin Hypercube sampling. [67] argues that the consensus of the metamodeling community is that space filling methods should be used for deterministic, non-random computer simulations. While these techniques are useful for creating a representative model across the space, they may not collect enough local information for constructing an accurate estimation of the feasibility boundary. It is therefore advisable to have a more directed approach to performing simulations in order to ensure that adequate local information is collected for accurately determining the feasibility boundary.

There are many possible models that can be applied to the collected experiments. Fitting a response surface is the traditional choice but more advanced mathematical models such as non-uniform rational B-splines (NURBs) and Kriging have successfully been applied to metamodeling applications [75, 44, 72]. While fulfilling the design criteria of giving both the design feasibility and feasibility boundary, statistical metamodeling assumes that a regular function can be fit to the highly complex mold filling behavior for polymer heat exchangers, for which it may not be feasible to do so. Advanced methods of sequential or adaptive sampling have been shown to improve the accuracy of statistical metamodeling [75, 60, 73], but they still rely on the application of regular functions and therefore may not be suitable for application to mold filling of polymer heat exchangers.

### 2.3.2 Classification Methods

Since the primary goal of this study is determining mold filling feasibility of a candidate design, classification techniques from the field of machine learning are a potential alternative to traditional metamodeling. Possible methods include Neural networks, Bayesian networks, decision trees, or Support Vector Machines (SVMs) [54, 14, 17]. These methods use complex learning techniques to devise a model for classifying a set of training data and advances in adaptive sampling have improved the usefulness of this training data and the accuracy of the developed model [22, 76]. While these methods provide a reasonable prediction of the feasibility of a candidate design, it provides only an implicit approximation of the feasibility boundary and therefore the precise location of the feasibility boundary is unknown, as represented in Fig. 2.1. Additionally, if the feasibility boundary is complex, the performance of classification techniques may degrade as designs approach the feasibility boundary. Therefore, while traditional classification techniques such as SVM could be applied to predict mold filling feasibility, they do not satisfy the design criterion of providing an explicit location of the feasibility boundary.

## 2.4 Problem Definition

This paper presents a new approach for explicitly constructing a moldability-based feasibility boundary for polymer heat exchangers. The proposed method takes inspiration from intelligent Design of Experiments literature and incorporates ideas from the active learning area to minimize the number of computational experiments

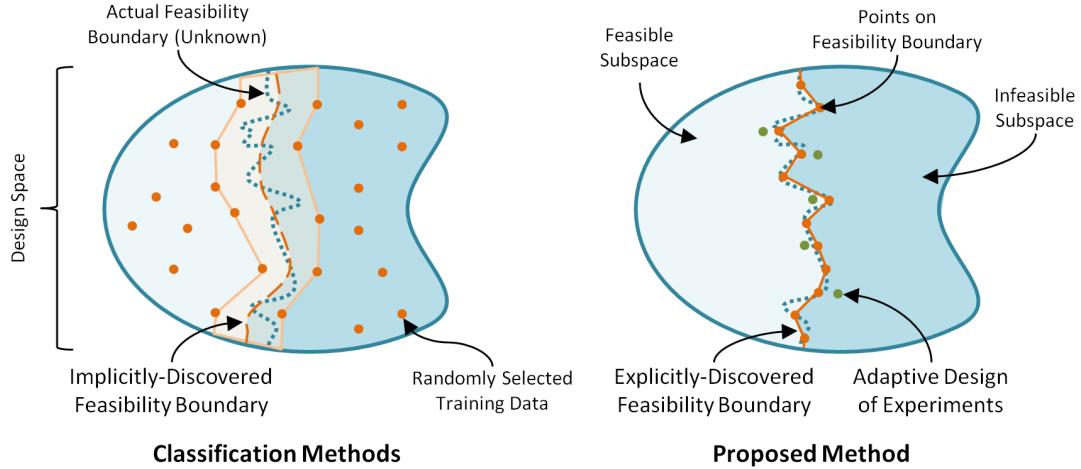


Figure 2.1: Comparison between classification methods and proposed method, noting implicitly vs explicitly discovered feasibility boundary and adaptive Design of Experiments.

needed to construct the feasibility boundary. This study utilizes an approach consisting of the following components:

- Rather than traditional sampling techniques, a method of adaptive DoE and sequential sampling is utilized to identify the feasibility boundary across the entire design space, as shown in Fig. 2.1.
- A design space of  $n$  variables is constructed with a grid of  $n - 1$  dimensions and a remaining search variable. At each grid position, the corresponding point on the transition region is found using adaptive search with the search variable.
- To reduce the number of computationally-expensive simulations required to develop the transition region, a method of feasibility boundary search is applied that uses previously found transition locations and the applied search pattern to predict the next transition locations and refine the search algorithm. These

methods are used to efficiently sample the design space to find transition locations across the entire space.

- Using the discovered transition region, a metamodel is applied to predict the transition location for a candidate design. This is used to determine feasibility and is a prediction of the location of the feasibility boundary.

This methodology is well-suited for predicting mold filling of polymer heat exchangers in design exploration or optimization frameworks and is demonstrated with a plate-fin polymer heat exchanger design, detailed in Section 2.5.3.

## 2.5 Approach

This study approaches the goal of developing a metamodel for mold filling of polymer heat exchangers by first developing a general method of adaptive DoE for multidimensional classification problems and then applying this method to the issue of mold filling for polymer heat exchangers. An algorithm for constructing an adaptive set of experiments to identify transition locations across the design space from which the transition region can be estimated, entitled the feasibility boundary search (Section 2.5.1) and transition point search algorithms (Section 2.5.2), is presented in the following sections and detailed in Fig. 2.2.

### 2.5.1 Feasibility Boundary Search Algorithm

**Step 1: Initialization.** The first step of the feasibility boundary search algorithm is initialization, a primary component of which is spatial partitioning: defining

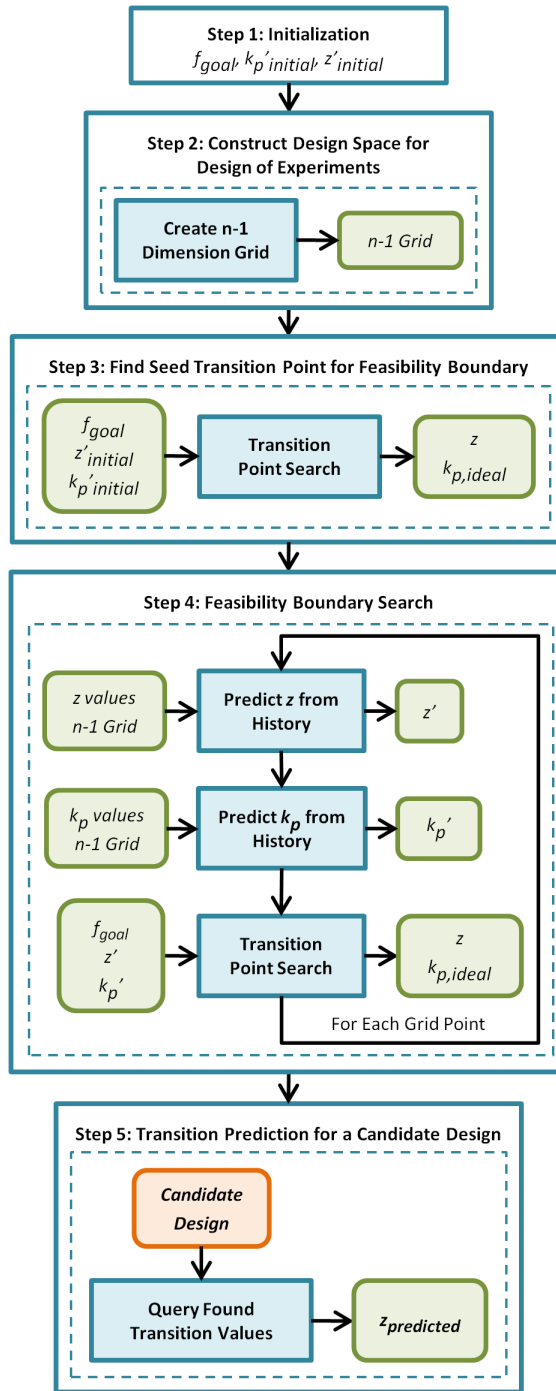


Figure 2.2: Flow diagram for the Feasibility Boundary Search Algorithm for predicting the location of the transition boundary for a candidate design.



using traditional factorial DoE techniques, as illustrated in Fig. 2.3. The remaining input variable is treated as the varying or search dimension and is used to find the transition point at each grid location across the design space. The design problem should be formulated such that the response value has a monotonic relationship with respect to the varying design dimension. This ensures a single transition location at each grid position, a requirement for the method presented in this study, and reduces the complexity of the transition point search method, presented in Section 2.5.2.

**Step 3: Find Seed Transition Point for Feasibility Boundary Search.**

With the design space defined, the location of the transition region is determined at an initial position in the design space, creating a seed transition point, as demonstrated in Fig. 2.3. At the first grid location, a full transition point search, described in Section 2.5.2, is completed with no prior knowledge of the response behavior and using arbitrary values for the necessary search parameters. This seed point and knowledge gained from performing the search is used by the feasibility boundary search component of the algorithm to improve the search efficiency for following locations in the design space.

**Step 4: Feasibility Boundary Search.** The primary component of the algorithm, a method of adaptive search termed feasibility boundary search, is used to improve the efficiency of the transition location search process at each grid location and therefore further reduce the number of computationally-expensive function evaluations required to define the transition region over the entire design space. By using previously found transition points and the search process used to find them, the feasibility boundary search method predicts the transition location at succes-

sive design positions and tunes the transition point search method utilized. In this way, information from the discovered transition region progresses as a frontier to the next grid locations and as the transition region is developed the searching process becomes more efficient. There are two primary components of the feasibility boundary search method: prediction of transition locations and adaptive control of the transition point search method.

**Step 4.1: Predict Transition Location.** From the seed point, the transition locations at the next grid points are predicted using constant extrapolation, as shown in Fig. 2.3. The next frontier of grid locations is predicted using linear extrapolation and the following locations are found using quadratic extrapolation. For this study, the maximum number of historical transition points used in the quadratic extrapolation method was set at three in order to reduce the distortion effects of the nonlinear mold filling behavior. As the predicted transition location approaches the actual transition location the search process becomes more efficient and fewer computationally-expensive simulations are required to find the transition location.

**Step 4.2: Adaptive Control.** The transition point search process utilizes certain control parameters that affect the rate of convergence for the search process, detailed in Section 2.5.2. As each search process is completed, it is possible to determine the value of the control parameters that would have led to immediate convergence, noted as  $k_{p,ideal}$  in Section 2.5.2. The feasibility boundary search component of the algorithm uses these ideal values to improve the search efficiency of the following locations and in this way improve the overall convergence rate for

identifying the transition region.

**Step 5: Transition Prediction of a Candidate Design.** With the feasibility boundary well defined from the adaptive DoE, post-processing and querying methods can be applied to estimate the feasibility of candidate designs. Possible post-processing methods include regression analysis, fitting a metamodel to the transition region, or applying SVM techniques to classify the feasibility subspaces. For a candidate design, the dimensions corresponding to the grid constructed in Step 2 are used with interpolation or other querying techniques to estimate the value of the varying dimension where the transition point occurs. This value is the explicit location of the feasibility boundary for the candidate design and is used to determine feasibility.

### 2.5.2 Transition Point Search Algorithm

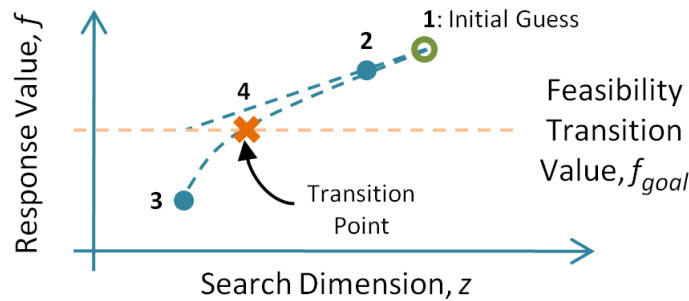


Figure 2.4: Transition Point Search Algorithm.

At each grid location, the goal is to find the transition location using minimal computationally-expensive function evaluations. For this study a method combining proportional control and interpolation methods, illustrated in Fig. 2.4, is utilized to

perform the search quickly and efficiently.

An initial guess is provided for each point, noted as  $z_{initial}$ , based on information from previous transition locations, as described in the feasibility boundary search algorithm. The initial guess is evaluated to find the corresponding response value, noted as  $f_{initial}$  or  $f_{prev}$ , and the error relative to the transition value,  $f_{goal}$ , and response function range,  $f_{range}$ , is calculated. Proportional control is applied to the calculated error to determine the next evaluation location,  $z_{next}$ , using Eqn. 2.1, with a proportional control constant of  $k_p$ . Next, with two known response values, linear interpolation is applied to determine the third evaluation location. Quadratic interpolation is then repeatedly applied until the convergence criterion is met. With the search complete, Eqn. 2.2 is applied to find the ideal proportional control constant,  $k_{p,ideal}$ , that would have led to immediate convergence to the found transition location,  $z_{transition}$ , for use in the feasibility boundary search algorithm.

$$z_{next} = z_{prev} + \left( k_p \frac{f_{prev} - f_{goal}}{f_{range}} \right) z_{prev} \quad (2.1)$$

$$k_{p,ideal} = \frac{z_{transition} - z_{initial}}{z_{initial}} \cdot \frac{f_{range}}{f_{initial} - f_{goal}} \quad (2.2)$$

For this method, the convergence criterion is defined as the transition value within a certain threshold or a minimum search resolution. The transition threshold is defined as the acceptable error in the calculated transition values and the minimum search resolution is used to ensure convergence and maintain design constraints on dimensional values.

Search constraints include design boundaries, which must be considered due to physical and design limits placed on the varying dimension. If the search extends

beyond the design boundaries, the transition location is assumed to be out of bounds due to the monotonic nature of the response function. Since the actual transition location is not known, the transition location is marked at the bound in these instances.

### 2.5.3 Problem Formulation Details

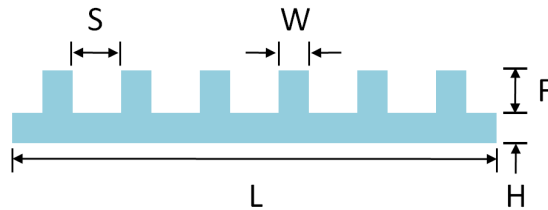


Figure 2.5: Plate fin design.

**Design Formulation.** A plate-fin heat exchanger design, the cross-section of which is detailed in Fig. 2.5, was chosen for the heat exchanger assembly due to its simple geometry and ability to be stacked in modules. There are five design variables for this configuration: Base length,  $L$ ; base thickness,  $H$ ; fin width,  $W$ ; fin height,  $F$ ; and fin spacing,  $S$ . Based on exploratory experiments, the design space for the plate-fin heat exchanger is presented in Tab. 2.1a.

The values for base thickness and fin width were chosen based on injection molding minimum and maximum thickness guidelines. The fin spacing was defined to ensure an adequate number of fins in the heat exchanger and the fin height was fixed at 10mm based on its limited effect on heat transfer performance observed in exploratory experiments. The minimum base length was set to ensure at least

Table 2.1: Problem formulation details.

(a) Design Dimensions

Design Variables		Min	Max	Grid Spacing
Base Length	$L$ , mm	200	800	100
Base Thickness	$H$ , mm	1	5	Varying
Fin Width	$W$ , mm	1	5	1
Fin Height	$F$ , mm	10	10	Fixed
Fin Spacing	$S$ , mm	3	15	3

(b) Material Properties for Selected Material

Material	Resin	Thermal Conductivity, W/m-K	Tensile Strength, MPa
PolyOne NJ-6000 TC Black	PA 12	10	110

approximately 1kW of heat transfer performance based on exploratory experiments and the maximum was set based on injection molding machine constraints.

**Material Selection.** The material selected for this application is PolyOne NJ-6000 TC Black, a commercially-available carbon-fiber filled Nylon 12. This material was chosen due to its balance of thermal and structural properties, its usefulness for injection molding applications, and the availability of a comprehensive set of material properties provided by the manufacturer for use in mold filling simulation. A selection of material properties for this polymer composite is shown in Tab. 2.1b.

**Simulation Methodology.** Moldflow<sup>®</sup>, the industry-leading finite element analysis tool for injection molding, was utilized to perform the mold filling simulation

for this study. Design selections include locating the injection gate in the center of the base plate, using steel mold construction, and utilizing a constant mesh density for all designs. Injection molding machine parameters were chosen using the default selection criteria provided with Moldflow<sup>®</sup> to correspond with industry standards based on overall part size and characteristics. These selections were chosen in such a manner that they reflect standard industry methods and ensure consistent results across the design space.

**Feasibility Boundary Search Parameters.** For this application, the transition response value is set to  $90\pm 1$  percent mold filling for which the design space will be separated into filled and unfilled subspaces. This value was selected based on the assumption that in cases within 10% of fully filled, adjustment of machine parameters, such as melt temperature and injection pressure, and mold design can be utilized to achieve a fully filled part. The response variable threshold is set to  $\pm 1$  percent filled to ensure that found transition locations are sufficiently close to the transition region.

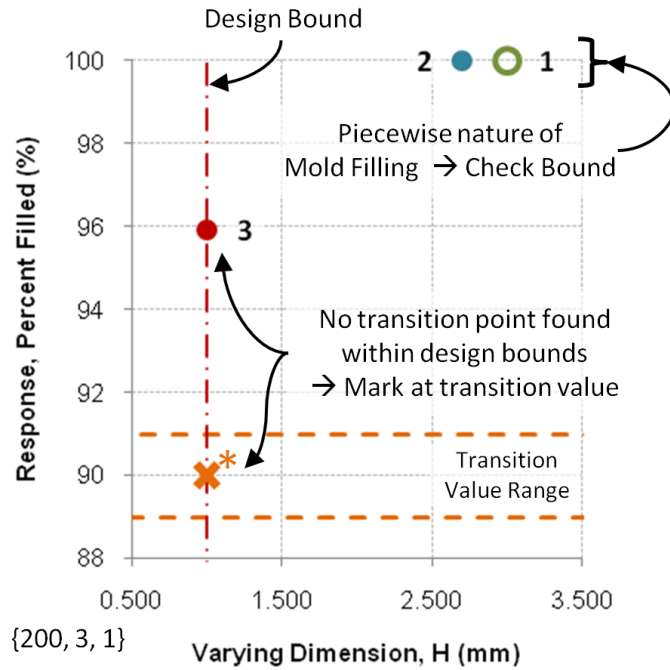
Table 2.1a also gives the grid properties selected for this analysis and indicates how the design space was divided according to the second step of the feasibility boundary search algorithm. It is recalled that a requirement of the transition point search process is that the varying dimension and response value should have a monotonic relationship. Base thickness was chosen as the varying dimension in this application due to the perceived relationship that mold filling monotonically increases as base thickness increases. This assumption is a result of the phenomenological relationship that as base thickness increases the flow resistance in the mold

decreases and the rate of cooling of the flow front decreases as well. These properties increase the flow length of the polymer melt and therefore mold filling increases monotonically with increasing base thickness.

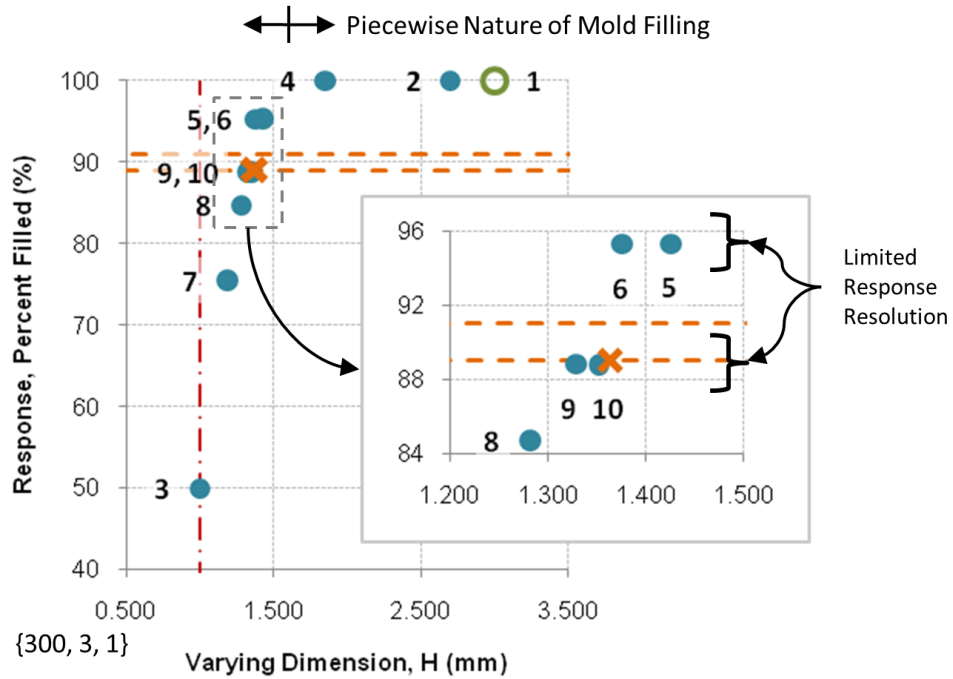
The minimum search resolution is set to 0.002mm for this study in order to ensure sufficient search iterations while not greatly exceeding the limit of typical machining capabilities. Finally, for this study a method of multi-linear interpolation was utilized to predict the transition point of candidate designs based on the discovered transition region.

**Selective Search Behaviors.** Several exploratory searches were performed to verify the performance of the developed transition point search strategy, outlined in Section 2.5.2. Results from these searches indicate that for this application certain selective search behaviors need to be introduced to ensure search convergence.

Points 1 and 2 in Fig. 2.6a and points 1, 2, and 4 in Fig. 2.6b indicate the piecewise nature of mold filling, with a continuous percent filled value for incompletely filled designs and a constant 100% filled value for completely filled designs. This poses difficulties in the employed search method due to undefined results for the interpolation methods when only completely filled values have been discovered. This is remedied with the introduction of selective search behaviors that check the lower design boundary when only 100% filled values have been found and which neglect 100% filled points in interpolation methods. Additionally, when only one point has been found below the transition region and only 100% filled values above the transition region, a method of biasing towards the lower value was used since only values below 100% filled are useful for approaching the transition value.



(a) Exploratory Transition Point Search Demonstrating Boundary Termination and Piecewise Mold Filling



(b) Exploratory Transition Point Search with Limited Response Resolution and Piecewise Mold Filling

Figure 2.6: Selective search behaviors.

Figure 2.6a demonstrates search terminating at a design boundary. Due to the assumed monotonic relationship between the response function and the varying dimension, if the search process reaches a design boundary and the transition point has not been found then the transition point is located beyond the design boundary. The exact transition location cannot be found due to design limitations and while the transition point could be estimated from known response values, for this study the transition point is set at the design bound. Additionally, Fig. 2.6b demonstrates the limited response resolution of the chosen simulation tool, with small changes in the varying dimension having minimal if no effect on the response value. This phenomenon is resolved with the use of the localized binary search and the minimum search resolution, which serves as a cutoff for the search process beyond which the response function does not respond.

## 2.6 Results and Discussion

The feasibility boundary and transition point search algorithms detailed in the approach section were applied for the given problem formulation in order to identify the transition region and determine the feasibility of candidate designs and the location of the feasibility boundary for finned plate polymer heat exchangers. A set of randomly selected test designs is then used to estimate the accuracy and usefulness of the developed model.

### 2.6.1 Transition Region Identification

Over the total design space of 175 grid locations, 803 function evaluations were required to define the transition region with the desired accuracy, with an average of 4.59 search iterations for each transition point, as shown in Table 2.2. The design boundary was reached for 31 grid locations and the transition point search converged due to reaching the minimum search resolution at 47 grid locations, indicating that the sensitivity of the mold filling simulation as a function of base thickness was dominating for some designs.

For comparison, exhaustive search was investigated to evaluate the search efficiency of the developed method. This method represents the more traditional approach to searching across a design space and could be used as an alternative to the developed method to find the transition location across the constructed design space.

Exhaustive search is assumed to use no adaptive sampling techniques and instead the varying dimension is uniformly divided across the design range. In order to achieve the same level of precision as the developed method, the minimum search resolution of 0.002mm should be used to divide the design space from 1 to 5mm, as defined in Tab. 2.1a. This creates 2,000 design levels for the varying dimension, which, when using the same grid of 175 positions for the remaining variables that was used in the developed method, leads to a total of 350,000 function evaluations for exhaustive search at the same precision as the developed method. Even if the spacing of the varying dimension is relaxed to ten times the minimum search resolution,

0.02mm, the total number of function evaluations required to (imprecisely) define the transition region is 35,000. Therefore, as detailed in Table 2.2, the developed method decreased the number of simulations required by nearly a factor of 436 when compared to the precise exhaustive search method, demonstrating the efficiency of the boundary search and transition point search algorithms in quickly and accurately identifying the transition region across the design space.

Table 2.2: Comparison of developed method and exhaustive search method.

Method	Avg. Search Iterations Per Transition Point	Total Function Evaluations	Factor Relative to Developed Method
Exhaustive Search	2,000	350,000	<b>435.87</b>
Developed Method	4.59	803	

## 2.6.2 Assessment of Prediction Performance

Due to the unknown nature of the response space, there are no methods to quantitatively measure the accuracy of the developed model. Instead, a significant set of varying test designs is used to develop a qualitative understanding of the developed model. For this study, 50 randomly selected heat exchanger designs were applied to get an understanding of the accuracy of the approach. These designs were selected using randomly chosen values within the design boundaries specified in Tab. 2.1a.

Of these 50 designs, the developed method successfully classified 100% of them. Of these designs, eight were found to be within 10% of the feasibility boundary,

indicating that they were the most difficult to classify and demonstrating the robustness of the developed approach. With the transition points discovered with the application of the developed method, multi-linear interpolation was applied in MATLAB<sup>®</sup> to determine the transition location for each design and therefore identify the feasibility boundary and classify the feasibility of the design. It was found that application of the developed method consumed 0.0469s of computation time to predict the transition location for all 50 test designs. The average Moldflow<sup>®</sup> simulation time required for each design was found to be approximately 35 minutes on a machine with a 2.83GHz Intel<sup>®</sup> Core<sup>™</sup> 2 Quad Processor and 8GB of RAM. Consequently, completing the simulations for the 50 test designs took nearly 30 hours of computing time. Therefore, the utilization of the developed method led to a dramatic reduction by a factor of approximately 2.24 million in computation time for predicting the feasibility and explicitly locating the feasibility boundary of candidate designs.

In addition to the 50 completely random tests used to test the overall prediction performance, a set of stress tests were designed using semi-random heat exchanger designs to demonstrate the effectiveness of the developed model in the most extreme cases. In this application, the most difficult cases to classify are those that are very close to the feasibility boundary and the stress tests were designed to specifically analyze the metamodel performance in this region. For the 50 stress test cases, all of the design criteria except for the base thickness were randomly selected. The feasibility boundary model was then used to calculate the base thickness where the feasibility boundary is located for each stress test case. Then the base thickness of

each stress test case was set at a randomly chosen value within the interval of  $\pm 10\%$  of the corresponding predicted feasibility boundary base thickness. The stress test cases are therefore only semi-random and are located very close to the feasibility boundary, representing the situation that is most difficult for the developed model to predict. Of the 50 stress test cases, the developed model correctly predicted 48 of them for a success rate of 96%.

While the stress test cases were designed to be the most difficult to classify and therefore some failures are to be expected, each failed stress test case, detailed in Table 2.3, was investigated further to analyze the underlying reasons the developed model may have failed. For Case 1, the actual mold filling of 91.48% is sufficiently near to the feasibility boundary design bound of 91% mold filling that it likely does not represent error in the identified feasibility boundary but instead potentially represents error that may have been introduced in the employed multi-linear interpolation prediction method. Case 2 is likely to have similarly failed due to the use of the rudimentary multi-linear interpolation prediction approach. Therefore, the underlying causes for both failed stress test cases is most likely not the accuracy of the collected feasibility boundary points but instead the employed prediction method that uses these collected points to estimate the location of the feasibility boundary for a candidate design and could be remedied with the use of a more advanced prediction method. The developed stress test represents the most difficult cases for the model classify and such a high overall success rate demonstrates the high accuracy and effectiveness of the developed feasibility boundary model and the utility of the feasibility boundary search approach for developing it.

Table 2.3: Failed Stress Test Cases (Units are mm).

<b>Case</b>	$L$	$W$	$S$	$H$	<b>Mold Filling</b>	$H_{Feasibility}$	<b>Predicted Feasibility</b>
1	365	2.2	13.0	1.2	91.48%	1.2465	False
2	528	1.0	9.0	1.8	86.51%	1.7738	True

## 2.7 Summary

The complex phenomena inherent in injection molding requires CAE simulation methods for predicting moldability but these methods are too intensive for use in applications where numerous trials are required, such as optimization or design exploration. Additionally, the requirement for minimal wall thickness in polymer heat exchangers necessitates an accurate estimate of the transition from a feasible to an infeasible design. The methods outlined in this study successfully identified the feasibility boundary, fulfilling the design goals and accurately predicting the moldability of finned plate polymer heat exchangers.

This study presents an adaptive DoE methodology that uses an adaptive sampling algorithm to explicitly locate the feasibility boundary between the feasible and infeasible subspaces of the design space. The application of traditional statistical metamodeling techniques in which a regular function is fit to a set of experiments was found to be unsuitable due to the complex nonlinear behavior inherent in injection molding. Classification techniques from the field of machine learning were considered but they offer only an implicit prediction of the feasibility boundary and therefore did not fulfill the design requirement of explicitly locating the boundary for use in optimization applications.

While the method utilized in this study was shown to be successful for a number of candidate designs, there are potential limitations and improvements that can be implemented. The use of a uniform grid when constructing the design space can introduce significant error into the constructed metamodel if the spacing is too coarse or important relationships between the design and response spaces are misunderstood. This can potentially be improved with the use of adaptive grid spacing or the introduction of multiple varying dimensions when constructing the design space. The feasibility boundary search process is important for reducing the required number of simulations to construct the transition region and the use of more advanced prediction techniques within the process, such as the application of machine learning methods, could lead to further improving the search efficiency. Finally, complexities inherent in the mold filling simulation, including the piecewise nature of mold filling and the limited response resolution to small changes in input parameters, introduced complications in the search process. The use of more advanced control schemes or search methods could improve the transition point search method and reduce the number of search evaluations needed to find transition points.

The utilized method employed adaptive search to locate points on the transition region while using minimal computationally-expensive simulations and as the transition region was discovered, a feasibility boundary search algorithm was used to improve search efficiency by predicting transition values and tuning search parameters based on previously found transition region information. The applied method was found to significantly reduce the number of required search iterations compared to an exhaustive search method and reduced the amount of computation time to pre-

dict the feasibility of 50 test designs from nearly 30 hours for Moldflow<sup>®</sup> simulation to less than 0.05 seconds for the applied method. The proposed method is therefore well-suited for applications such as design exploration and optimization and was successfully utilized to accurately predict the feasibility of candidate polymer heat exchangers designs.

## Chapter 3

### Feature Removal for Efficient Assessment of Mold-Filling Feasibility of Finned-Plate Geometries

#### 3.1 Introduction

While metamodeling techniques are incredibly powerful for quickly predicting certain phenomena, they may not be flexible enough to be applied for changing design criteria. As the potential heat exchanger geometry becomes more complex and design changes are introduced, a mold filling metamodel may not be suitable since it is developed based on a particular design. In these instances, another approach for predicting filling behavior may be necessary.

This chapter presents a model simplification approach for predicting mold filling of finned-plate heat exchanger geometries through the use of a reduced complexity model that will potentially decrease simulation time while maintaining prediction accuracy. The developed approach uses an equivalent flat plate to represent the finned geometry and a metamodel for flat plate mold filling to remove the requirement for simulation of finned geometries and therefore significantly reduces the computation time required to predict mold filling. This approach is then evaluated for a set of randomly generated finned-plate designs to determine its effectiveness for varying geometries.

## 3.2 Background

Model simplification is a technique of altering the original computer-aided design (CAD) model for simulation such that complexity, and therefore simulation time, is decreased while introducing minimal error in simulation predictions compared to actual behavior. Examples of model simplification approaches include identifying and removing non-critical design details, replacing complex features with simplified geometry, or altering mesh characteristics to simplify represented geometry. Additionally, the complex design may be reduced to a simple design for which a metamodel exists, thus removing the need for simulation and further reducing the computation time needed for simulation predictions. Model simplification is useful for many Finite Element Analysis (FEA) applications, especially those in which complex behaviors necessitate computationally-expensive simulation and where reducing simulation time could improve the utility of applications such as design exploration or optimization.

## 3.3 Related Work

Based on the classification proposed by [70], the model simplification process can be divided into the following four types of operators: surface entity based, volume entity based, explicit feature based, and dimension reduction based. These types are explained in detail below and selecting a model simplification technique is based on a number of factors unique to each application, including model geometry, analysis method, system conditions, and other considerations.

In surface entity based model simplification, the surface features of the geometry guide the model simplification approach. There are three primary techniques based on surface entities: Low pass filtering, Face cluster simplification, and Size based entity decimation. Low pass filtering is limited to 2D geometry and removes details based on a frequency representation of the original geometry, with it stated that high frequency terms represent detailed features [51]. In face cluster simplification, the faces of adjacent mesh elements are clustered and, based on defined metrics, are collapsed to form a merged face [65, 66, 38]. This approach preserves the geometry of the original model and serves to reduce the amount of elements needed to define the overall geometry. Finally, in size based entity decimation the geometry is expressed as an explicit volumetric representation in terms of cells. The size of these cells and the edges contained within them are ranked by size, which is used to remove detailed features that fall below a defined size threshold [45, 46, 47, 31]. This approach is useful due its generalized implementation and control over parameters such as the introduced geometrical error.

For volume entity based model simplification, Voxel based simplification and effective volume simplification are the the two most predominant methods. Voxel based simplification is useful for simplifying features such as holes and small protrusions based on part geometry that falls predominantly within or outside of the core geometry [3, 34]. Effective volume simplification is useful for creating multi-resolution models for varying analysis requirements that can remove features based on varying levels of detail [48, 49, 50].

Explicit feature based model simplification techniques define a class of explicit

features, often defined by the particular application, such as manufacturing or FEA, evaluate the model, and evaluate defined metrics based on which simplification decisions are made. There are three primary forms for this approach to simplification: Prismatic feature, Blend feature, and Arbitrary shaped features. Prismatic feature simplification is utilized to identify and remove features such as blind holes, through holes, bosses from the original geometry [19, 18]. Blend feature simplification is primarily aimed at removing fillet and round features from the original geometry and is often used to prepare models for further feature-based model simplification techniques [78, 69]. Finally, arbitrary shaped features simplification is useful for identifying and removing feature faces that correspond with a defined feature, typically protrusion or depression feature types, and patching the hole that is created [74, 41]. This is the most general form of explicit feature based simplification and is especially useful when a rule-based approach is applied to remove a large variety of features based on inherent geometrical properties.

Dimension reduction based simplification has the potential of dramatically reducing the computational intensity of performing analyses such as FEA by reducing CAD models to 2D or, potentially, 1D models and subsequently reducing geometrical complexity. Medial axis transform, one of the most well established approaches to dimensional reduction, is performed using the following three steps: Delaunay triangulation of the object is performed, circum-circles for each triangle are determined, and a curve is fitted to the circum-centers, forming the medial axis, an example of which is shown in Figure 3.1 [4, 24, 68, 30]. The original physical and system properties are then transformed and applied to the reduced-dimension

medial axis. This approach is useful for potentially reducing geometrical complexity while retaining the general properties of the original geometry but has limited applicability based on geometric and application considerations.

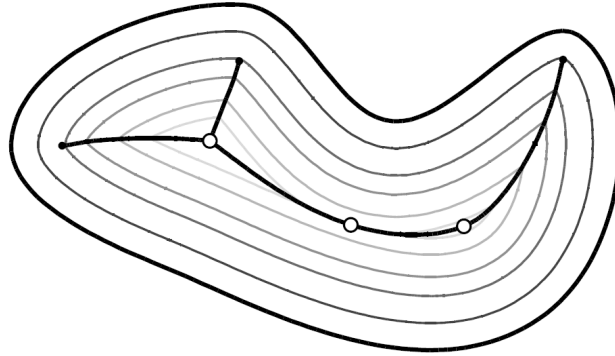


Figure 3.1: Example medial axis transform of shape whose boundary is the outer closed curve. [4]

### 3.4 Problem Definition

This study is interested in the use of model simplification techniques to decrease the simulation time for predicting the mold filling behavior of plate-type polymer heat exchanger geometries and, in general, finned-plate geometries. This approach will approximate the filling behavior of a given finned-plate geometry by determining an equivalent simplified geometry, in this case a flat plate representation, and performing the mold filling simulation for the simplified geometry. To further reduce the computational intensity of the mold filling prediction process, the use of a flat plate mold filling metamodel will be investigated. This technique will be demonstrated for a representative finned-plate geometry and then applied to

generalized finned-plate test cases to determine the suitability of this approach.

## 3.5 Approach

### 3.5.1 General Flat Plate Mold Filling Metamodel

The model simplification approach employed in this study uses a flat plate model to represent the simplified geometry that can dramatically reduce the complexity of finned-plate designs. The need for simulation can be removed entirely if a metamodel for mold filling in flat plate geometries can be created, further reducing the computation time required to predict mold filling of finned-plate geometries.

In order to be flexible to a variety of geometries and processing conditions, an overarching metamodel for flat plate mold filling was developed to demonstrate the potential usefulness of this approach. This metamodel considered plate dimensions and processing conditions as independent variables and the chosen values are detailed in Table 3.1. Constants include setting the mold temperature based on recommended setting for the selected material, utilizing a center injection gate, and simulation variables such as mesh density. This metamodel was constructed using a traditional factorial Design of Experiments technique and a model was fitted using regression techniques to predict the filled radius,  $r$ , from the center gate as a measure of mold filling. Additionally, three materials (detailed in Table 3.2) were chosen to identify common trends between them and ensure the developed metamodel had a form that corresponded with observed physical behavior.

Using the design cases studied, each variable was examined while keeping the

Table 3.1: Design variables for general flat plate mold filling metamodel.

<b>Parameter</b>	<b>Value</b>	<b>Spacing</b>	<b>Units</b>	<b>Variable</b>
Plate Thickness	1-10	1	mm	$H$
Injection Pressure	150-180	10	MPa	$P$
Injection Flow Rate	4500-5000	100	cm <sup>3</sup> /s	$Q$
Melt Temperature (PolyOne)	250-277	10	°C	$T$
Melt Temperature (ABS / PP)	200-230	10	°C	

Table 3.2: Materials studied for general plate filling metamodel.

<b>Material Name</b>	<b>Matrix Material</b>	<b>Filler Material</b>
PolyOne NJ-6000 TC Black	Nylon 12	Carbon Fiber
ABS Generic Estimate	ABS	None
PP Generic Estimate	Polypropylene	None

other variables constant to understand the relationship between each variable and the filled radius. The results are shown in Figures 3.2 and 3.3 with the fixed variables noted and the results given for each material. Based on the measured trends, the relationships detailed in Equation 3.1 were determined.

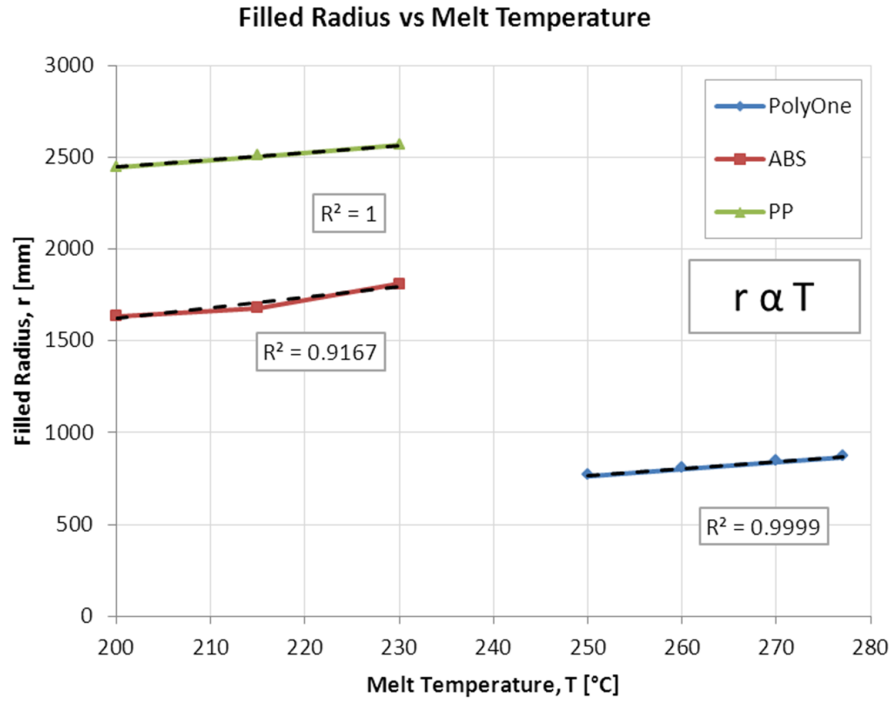
$$r \propto T$$

$$r \propto Q$$

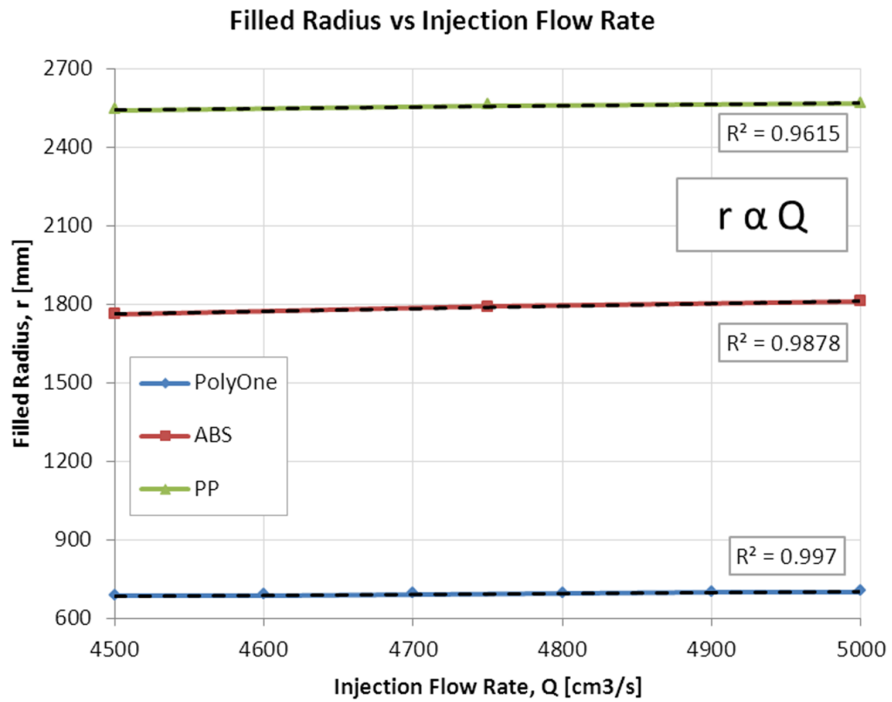
$$r \propto P$$

$$r \propto H^{1/2} \tag{3.1}$$

Based on the determined physical relationships between the input variables and the filled radius, the general flat plate filling metamodel was defined in the form expressed in Equation 3.2 with the potential of expanding it to other materials with

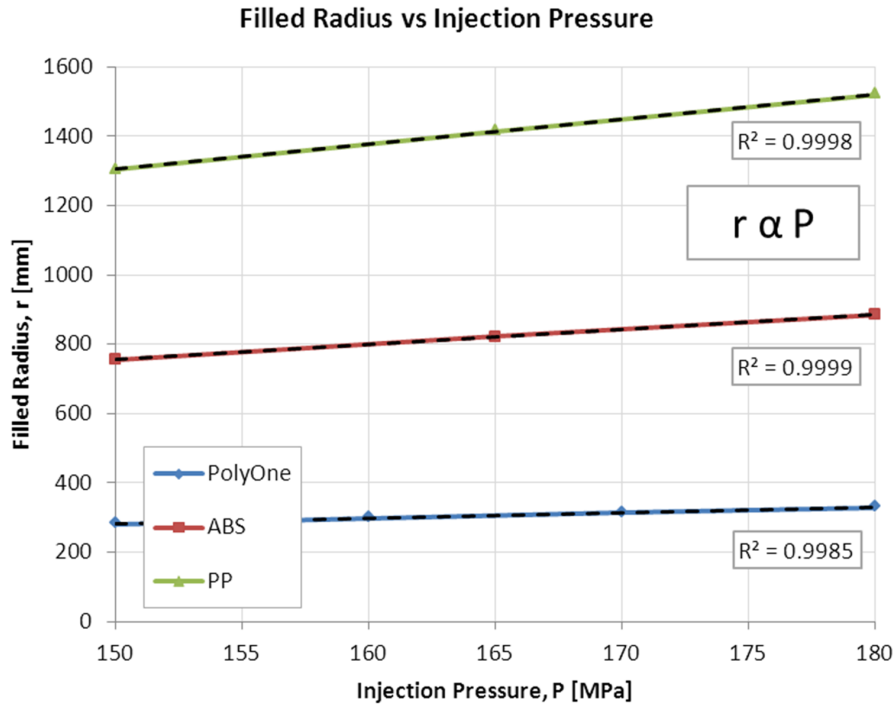


(a) Flat plate mold filling metamodel trend, temperature.

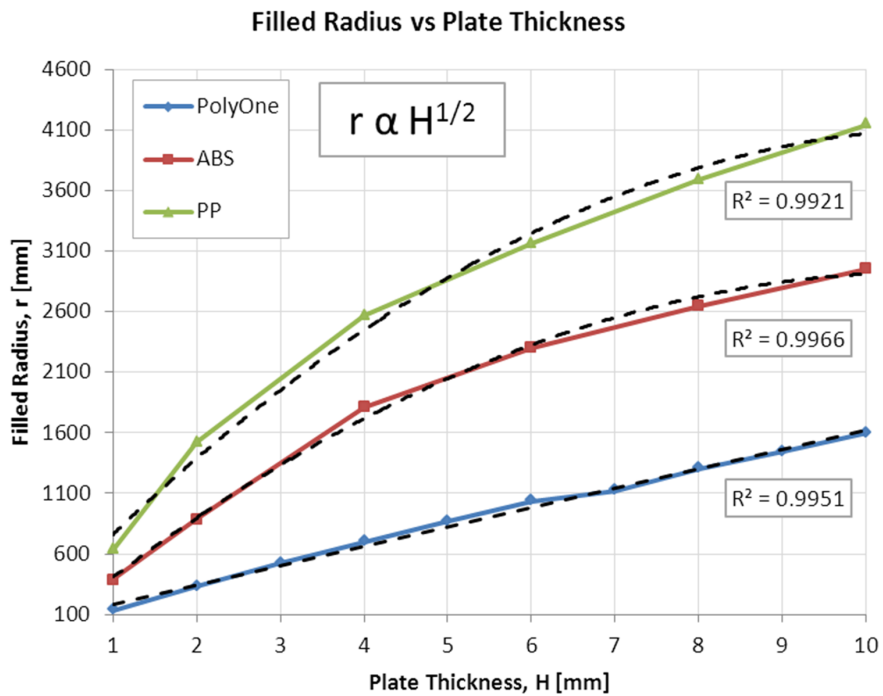


(b) Flat plate mold filling metamodel trend, flow rate.

Figure 3.2: Flat plate mold filling metamodel trends.



(a) Flat plate mold filling metamodel trend, pressure.



(b) Flat plate mold filling metamodel trend, thickness.

Figure 3.3: Flat plate mold filling metamodel trends, continued.

the addition of viscosity term. For this application, the metamodel was developed for only the goal material, PolyOne NJ-6000 TC Black, using the form shown in Equation 3.2. A regression analysis was used to find the metamodel that best fit the 120 training datapoints and the developed metamodel shown in Equation 3.3.

$$r = kTQPH^c \quad (3.2)$$

$$r(T, Q, P, H) = 6.0819 \times 10^{-7} TQPH^{1.0655} \quad (3.3)$$

While this model was shown to have reasonable accuracy, with an average error of 0.27%, it had high levels of deviation, especially in regions with relatively small base thicknesses. In order to reduce the overall error of the model and reduce the variance, the model was split based on base thickness. This isolates any unaccounted for behavior at varying base thicknesses but could lead to additional complexity if the model becomes too fragmented. Based on an exploratory study, splitting the metamodel into three components successfully reduced overall error from 0.27% to 0.05% and significantly reduced the error variance, as shown in Table 3.3. The final form of the general flat plate mold filling metamodel is shown in Equation 3.4.

$$r(T, Q, P, H) = \begin{cases} 5.3493 \times 10^{-7} TQPH^{1.3358} & H \leq 2 \\ 6.9813 \times 10^{-7} TQPH^{1.0156} & 2 < H \leq 5 \\ 8.8125 \times 10^{-7} TQPH^{0.8723} & H > 5 \end{cases} \quad (3.4)$$

Finally, a set of test points were used to test the accuracy of the developed general flat plate mold filling metamodel. These test points were chosen based on points of interest for the model simplification approach and to reflect design parameters

Table 3.3: Reduction in model error by splitting general flat plate metamodel by base thickness.

<b>Equation Form</b>	<b>Error</b>		
	<i>Avg</i>	<i>Max</i>	<i>Min</i>
Single Equation	0.27%	19.49%	-13.60%
Split Equation	0.05%	6.75%	-8.45%

that would be employed for that study. Therefore, the melt temperature, injection flow rate, and injection pressure were fixed, shown in Table 3.4, with a varying base thickness. The results of these test points showed a maximum prediction error of 2.51% and an average of 1.95%, as detailed in Table 3.5. The developed metamodel therefore demonstrates a reasonable level of accuracy and shows strong potential for use in a model simplification application.

Table 3.4: Fixed parameters for test points for general flat plate mold filling metamodel.

<b>Parameter</b>	<b>Value</b>	<b>Units</b>
Injection Pressure	180	MPa
Injection Flow Rate	5000	cm <sup>3</sup> /s
Melt Temperature	277	°C

### 3.5.2 Localized Flat Plate Mold Filling Metamodel

While the developed general flat plate mold filling metamodel is useful for demonstrating the potential usefulness of this model simplification approach, a more accurate local model was developed for precisely identifying the underlying model simplification behavior and generating the subsequent relationships. This model

Table 3.5: Test points for general flat plate mold filling metamodel.

<b>H,mm</b>	$r_{filled}$ , mm	$r_{calc}$ , mm	<b>% Error</b>
4.2	734.66	747.53	1.72%
4.4	769.87	783.70	1.76%
4.6	801.15	819.89	2.29%
4.8	835.31	856.11	2.43%
5.2	902.28	925.53	2.51%
5.4	937.51	956.51	1.99%
5.6	972.24	987.34	1.53%
5.8	1003.75	1018.03	1.40%
AVG			1.95%

constrains all of the processing parameters, the values of which were shown previously in Table 3.4, and the majority of the flat plate geometry leaving only the plate thickness variable. Additionally, a localized range of plate thicknesses was examined to limit the developed metamodel to only the studied area and ensure a strong local correlation.

The collected plate values and the developed local metamodel are shown in Figure 3.4 with the quadratic metamodel overlaid. The metamodel was found to have an  $R^2$  value of 0.9965 and an average error of 0.02%. This model is extremely useful in the development of model simplification techniques because it allowed optimization and other methods to be applied with high level of accuracy to quickly develop an understanding of the model simplification behavior and its possible applications.

$$V_{filled} = 8.591 \times 10^5 H^2 - 2.409 \times 10^6 H + 2.156 \times 10^6 \quad (3.5)$$

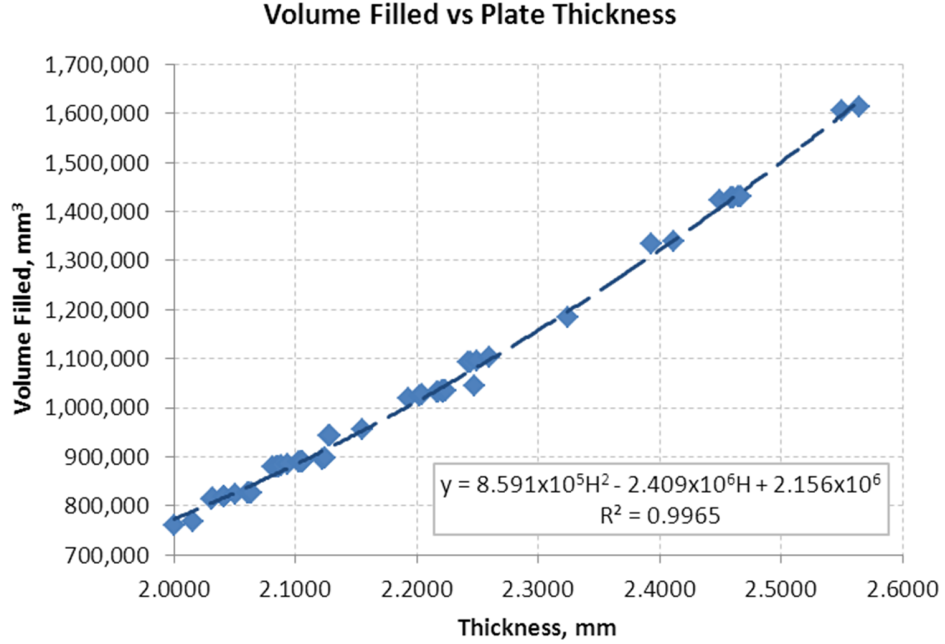


Figure 3.4: Localized flat plate mold filling metamodel.

### 3.5.3 Model Simplification - Disc-Fin Model

With the flat plate mold filling metamodel successfully developed, a case study with a disc-fin geometry was used to analyze the effectiveness of a model simplification approach for general finned plate geometries. This disc-fin geometry, shown in Figure 3.5, was chosen due to its high level of control over fin properties and even filling behavior allowing for isolation of the effect of fins on filling behavior. The following dimensions were varied in the disc-fin geometry: inner fin radius, fin height, and fin width.

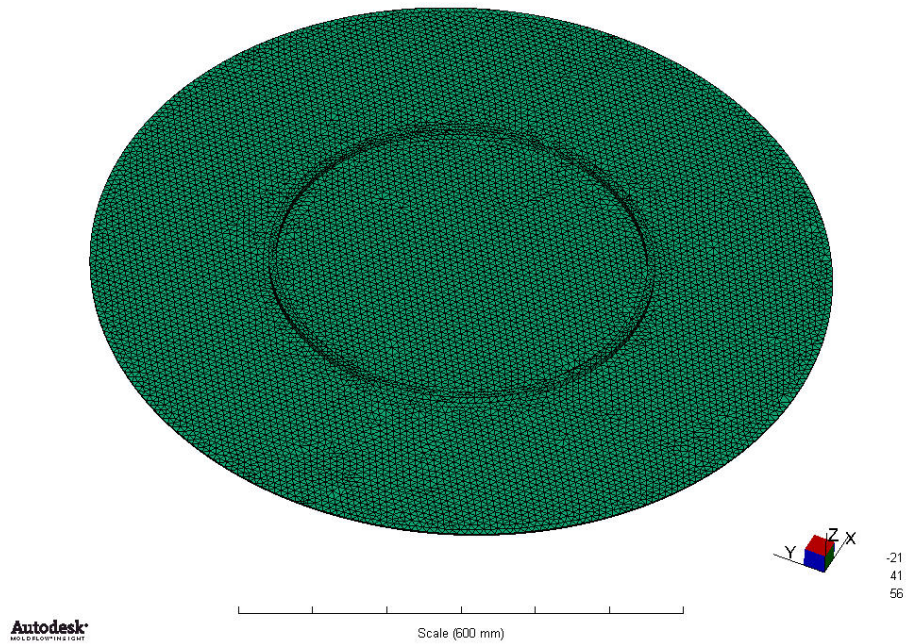


Figure 3.5: Disc-fin geometry.

Test cases were selected from across the sample space to ensure wide applicability of the developed model simplification technique and to develop an understanding of conditions where model simplification techniques are not suitable. The selected design criteria, shown in Table 3.6, were chosen to examine a wide range of fin volume concentrations at differing fin spread and size. The relative fin size was defined as *short* by fixing the fin width to 4mm for cases with fin concentrations from 2-10% and 8mm for cases with fin concentrations from 20-30% and then setting the fin height such that the desired fin concentration level was met. Similarly, *tall* fins were defined by a fin height set at 40mm and a fin width set to reach the defined fin concentration. This approach allows varying fin shapes to be tested independently

of overall fin size or volume. Each test case was then simulated using Moldflow<sup>®</sup> to determine the actual mold filling response, which was then used, along with the geometry properties of each design, in the development of the model simplification approach.

Table 3.6: Disc-fin design criteria for test cases.

<b>Parameter</b>	<b>Values</b>
Fin inner diameter	150mm, 300mm, 500mm
% Fins (By Volume)	2%, 5%, 10%, 20%, 30%
Relative Fin Size	<i>Short, Tall</i>

With the actual mold filling behavior understood for each test geometry, a method of approximating this filling behavior with a flat plate geometry was examined. There are only two variables that can be controlled for this flat plate geometry: plate thickness and plate diameter. In performing the mold filling simulation, Moldflow<sup>®</sup> makes injection molding machine sizing decisions based on the specified processing parameters and the overall cross-sectional area of the geometry. This means that in order for the machine sizing to be equivalent for the disc-fin geometry and its flat plate approximation, the overall cross-sectional area must be the same for both. Therefore, the flat plate diameter is set equal to the corresponding disc-fin diameter and the only variable that can be controlled to affect mold filling behavior is the plate thickness.

In order to approximate the mold filling behavior of the original disc-fin geometry, a scaled thickness value must be calculated. There were four dimensions from the disc-fin mold filling results that could be used to determine the scaled thickness

value:  $r_{Total}$ ,  $V_{Total}$ ,  $r_{Filled}$ ,  $V_{Filled}$ . With these dimensions, shown in Figure 3.6, the *Total* values represent inherent geometry dimensions, and the *Filled* values are more useful since they represent the actual mold filling behavior of the geometry. In order to determine the scaled thickness value, a disc with radius of  $r_{filled}$ , calculated using Equation 3.6, and volume of  $V_{filled}$  was assumed to represent the geometry and the subsequent thickness value was calculated. This approach is detailed in Equation 3.7, with the introduction of a tuning coefficient,  $k$ , which will be used to refine the fit of the model to the collected disc-fin data.

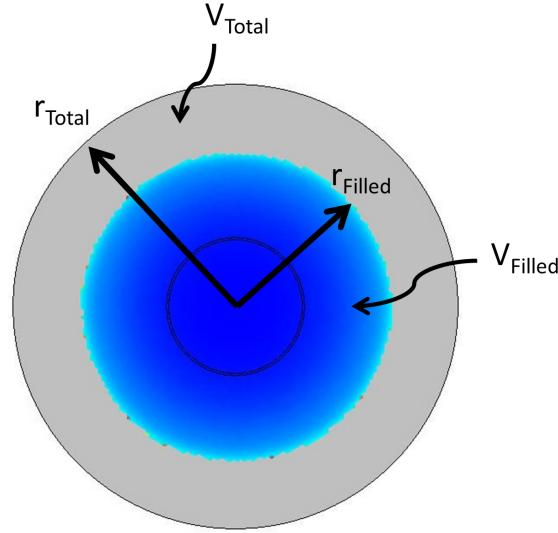


Figure 3.6: Model simplification details.

$$r_{filled} = \sqrt{\frac{(V_{filled} - V_{fins})}{\pi H}} \quad (3.6)$$

$$H_{scaled} = k \left( \frac{V_{filled}}{\pi r_{filled}^2} - H_{orig} \right) + H_{orig} \quad (3.7)$$

Figure 3.7 shows the percent error between the measured mold filling for the disc-fin test cases and the scaled thickness flat plate with no tuning factor ( $k = 1$ ).

These results, in addition to demonstrating the need for a tuning factor, show a strong correlation between the various test cases at each fin concentration level, indicating that a unified model simplification approach should be successful rather than having to split the approach based on geometry values. Figure 3.8 displays the results of introducing various arbitrary tuning factors ( $k = 0.75, 0.50, 0.25$ ) and the resulting decrease in overall error of the scaled thickness flat plate approximation. An ideal tuning factor was determined by minimizing the average error across all of the test cases and was calculated as  $k = 0.293$  with an overall average error of 0.02%. The results of applying this ideal tuning factor are shown in Figure 3.8. The developed scaled thickness flat plate approximation model shows a strong correlation to the actual disc-fin results and is used as the basis for the more general model simplification approach for finned-plate geometries.

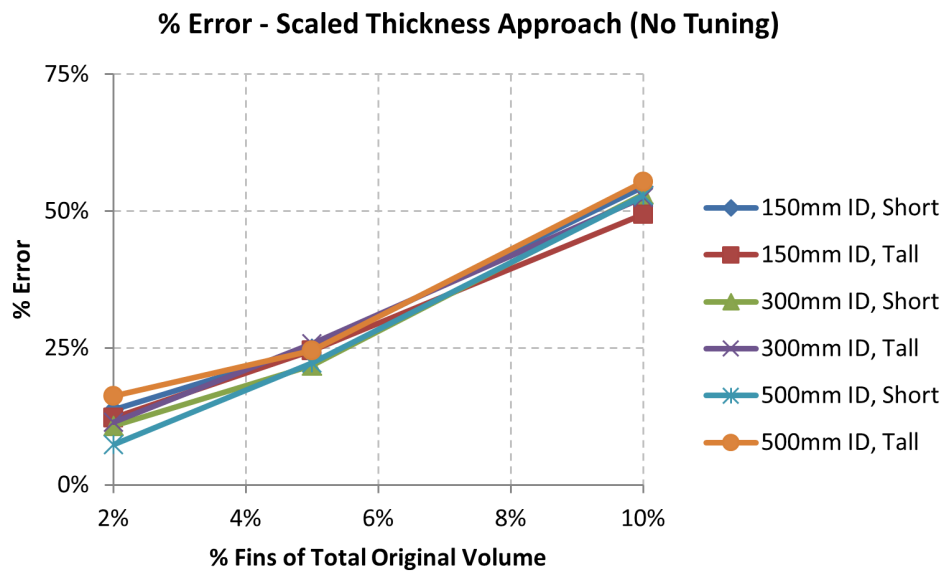


Figure 3.7: Scaled thickness flat plate simplification results with no tuning factor.

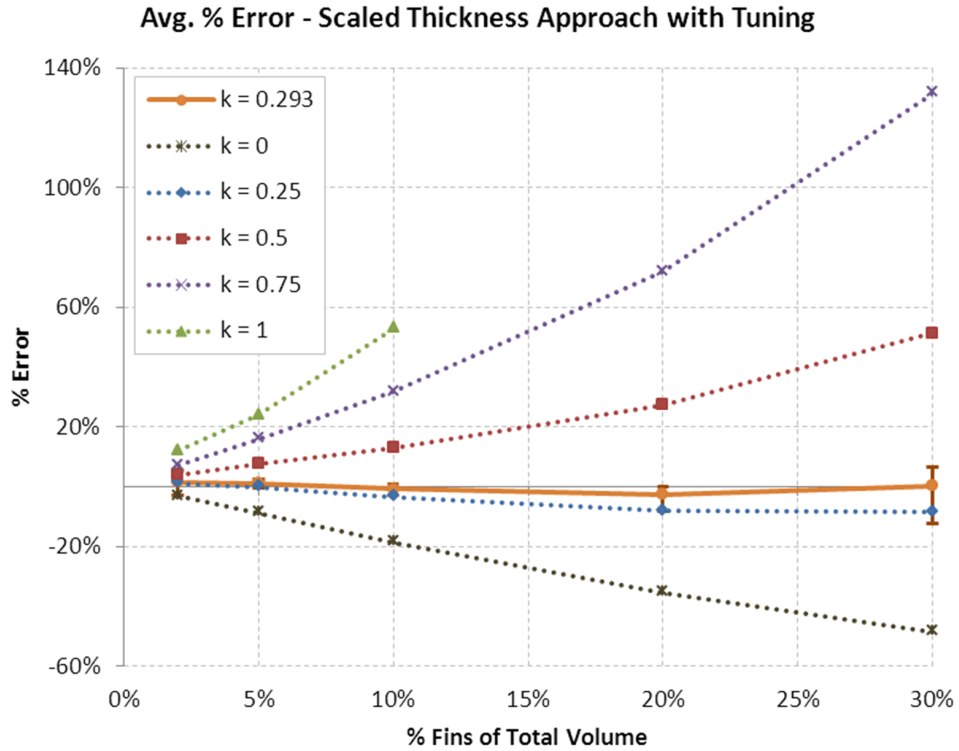


Figure 3.8: Application of tuning factors, including an ideal tuning factor.

### 3.6 Results and Discussion

In order to test the effectiveness of the developed flat plate model simplification technique, a set of randomly selected test cases were applied. These test cases used a set of randomly generated fins over a variety of fin volume concentrations in order to best measure the overall effectiveness of the model and determine the robustness of the approach and for which design regions it is suitable.

Figure 3.9 shows an example of the test finned plate geometry. The plate dimensions correspond with those used in the localized flat plate model and the fins are randomly generated based on the design criteria shown in Table 3.7. Four sets of

five test cases were developed at fin volume concentrations falling into the following general fin concentration categories: 5%, 10%, 20%, > 20%.

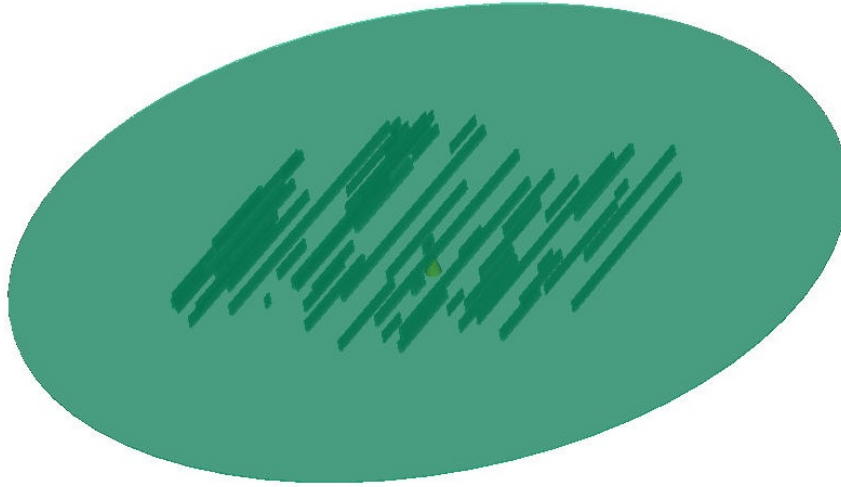


Figure 3.9: Example of randomly-generated finned-plate design.

Table 3.7: Design criteria for randomly-generated finned-plate designs.

<b>Parameter</b>	<b>Value (mm)</b>
Base Diameter	1000
Base Thickness	2
Fin Width	1-10
Fin Height	10
Fin Length	> 10
Fin Spacing	> 2

The 20 test cases were simulated in Moldflow<sup>®</sup> and the results were compared with the predictions from the developed flat plate model simplification technique. The complete results are shown in Table 3.8 and Figure 3.10 shows the relationship between the fin volume concentration and the percent error between the model

simplification prediction for mold filling and the Moldflow<sup>®</sup> results.

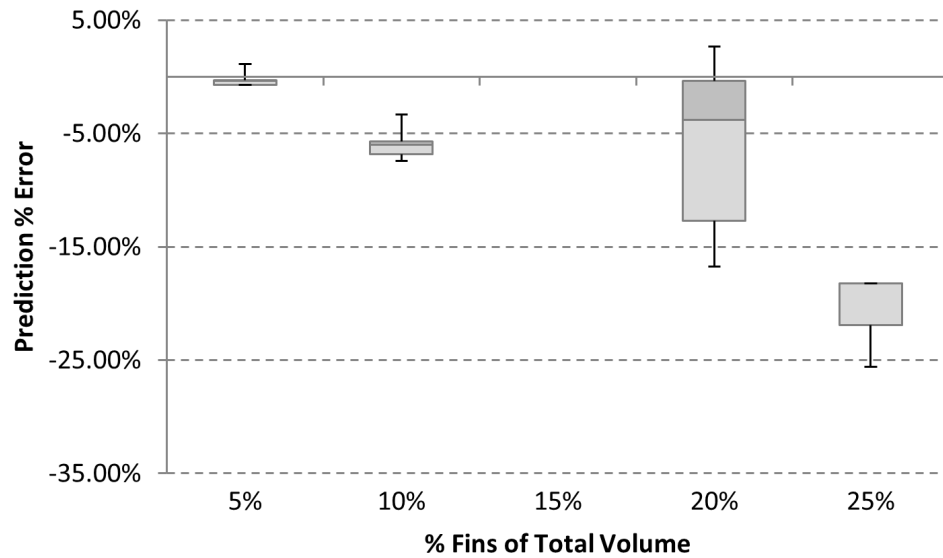


Figure 3.10: Model simplification results.

Based on the findings of the 20 test designs, this model simplification technique shows minimal error for geometries with fin volume concentrations less than 10% and is applicable for geometries with up to 20% fins by volume. The average error biasing of underestimating the volume filled can be potentially reduced with refinement of the tuning parameter but is useful for ensuring a conservative estimate of mold filling. The large average error and deviation above fin volume concentrations of 20% demonstrates the limits of the developed flat plate model simplification method as the mold filling behavior in the fins begins to dominate the overall filling behavior of the geometry.

To relate the usefulness of the developed method to a plate-fin heat exchanger application, optimal heat exchanger designs were analyzed to determine the percent

Table 3.8: Complete results for the investigated test cases.

ID	Total Volume	Fin Volume	% Fins	Volume Filled	Predicted Volume Filled	% Error
1	1,645,526	74,730	4.54%	837,737	834,925	-0.34%
2	1,659,596	88,800	5.35%	853,032	847,061	-0.70%
3	1,663,016	92,220	5.55%	845,151	851,616	1.12%
4	1,672,586	101,790	6.09%	864,727	858,693	-0.70%
5	1,687,271	116,475	6.90%	875,188	872,487	-0.31%
6	1,707,701	136,905	8.02%	952,897	882,419	-7.40%
7	1,707,881	137,085	8.03%	940,701	884,389	-5.99%
8	1,709,711	138,915	8.13%	939,999	886,375	-5.70%
9	1,730,756	159,960	9.24%	940,147	908,930	-3.32%
10	1,758,071	187,275	10.65%	996,299	928,254	-6.83%
11	1,848,596	277,800	15.03%	1,014,879	1,041,845	2.66%
12	1,925,786	354,990	18.43%	1,136,599	1,107,297	-2.58%
13	1,930,196	359,400	18.62%	1,150,976	1,107,168	-3.81%
14	1,952,141	381,345	19.53%	1,219,893	1,107,810	-9.19%
15	1,955,711	384,915	19.68%	1,291,161	1,081,947	-16.20%
16	1,958,336	387,540	19.79%	1,140,143	1,161,222	1.85%
17	1,969,556	398,760	20.25%	1,311,921	1,092,170	-16.75%
18	2,090,546	519,750	24.86%	1,461,292	1,195,212	-18.21%
19	2,144,351	573,555	26.75%	1,522,061	1,244,880	-18.21%
20	2,170,481	599,685	27.63%	1,638,279	1,218,940	-25.60%

fin volume of total volume. [53] optimized the plate-fin heat exchanger geometry based on the total coefficient of performance, incorporating thermal performance and energy efficiency, and the optimum designs are Cases A and B in Table 3.9. [15] included injection molding considerations in determining the optimum heat exchanger design, using metrics such as manufacturing costs, labor costs, pumping energy, and thermal performance for optimization. Cases C, D, and E in Table 3.9 are the resulting optimum heat exchangers at varying parametric values. Based on the selected designs, the developed model is useful for Cases A and B, but is unsuitable for Cases C, D, and E. Therefore, the approach may have to be expanded in order to cover the entire range of percent fin volume of total volume that may potentially be found in plate-fin heat exchanger designs.

Table 3.9: Example plate-fin heat exchanger designs from optimization studies.

Case	L (mm)	H (mm)	F (mm)	S (mm)	W (mm)	Fin Volume / Total Volume
A	1,000	1.0	8.5	133	0.765	4.35%
B	1,000	1.0	11.6	92.7	1.486	14.70%
C	872	3.52	10	3	2.58	56.73%
D	800	3.28	10	3	2.36	57.27%
E	912	3.73	10	3	2.44	54.50%

### 3.7 Summary

The need for flexibility to potential design changes necessitates the use of a more generalized technique that is robust to design variations and can be used in

situations that a specialized metamodel may be unsuitable. Model simplification is an approach for reducing simulation time by applying a variety of techniques for decreasing the complexity of CAD designs while maintaining the quality of the simulation results. This chapter presents a model simplification approach for estimating the mold filling behavior of general finned plate designs with an equivalent flat plate model and flat plate mold filling metamodel.

A flat plate mold filling metamodel was investigated and both a general and localized metamodel were developed. The general metamodel is useful for a range of plate design criteria and processing parameters and the localized metamodel was used for the development of the model simplification technique due to its high level of accuracy in the region of interest. A disc-fin geometry was used to measure the effects of general fin properties on filling behavior and was used to refine and optimize the flat plate model simplification approach to best represent identified behavior. A set of randomly-generated finned plate designs were then used to evaluate the developed model simplification technique and it was shown to have sufficient accuracy for fin concentrations less than 20% and was unsuitable for higher fin concentrations.

This study successfully developed a model simplification approach for representing finned plate geometries with an equivalent flat plate and applying a flat plate mold filling metamodel. This approach is useful due to its flexibility with a variety of finned plate geometries and can be used in applications such as evaluating new heat exchanger designs and understanding the effects of processing parameters on finned plate mold filling performance.

## Chapter 4

### Development of a Fiber Orientation Measurement Methodology

#### 4.1 Introduction

In thermally-enhanced and other fiber-filled composites, fiber orientation can play an important role in determining the material properties of created parts. Thermally-enhanced fibers exhibit thermal and structural properties that are order of magnitudes higher along the length of the fiber compared to transverse to the length of the fiber. Therefore fiber alignment can lead to anisotropic material properties that must be accounted for in the design stage. In injection molded parts, many factors affect fiber alignment, including the geometry of the part and injection molding processing parameters, such as melt flow rate. Figure 4.1 below demonstrates the fiber orientation process that must be understood in order to properly design for fiber orientation in injection molded parts in order to reach desired performance goals.

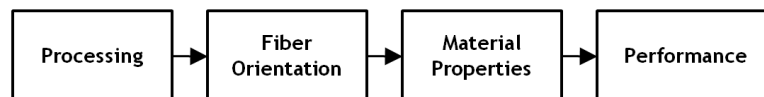


Figure 4.1: The effect of processing parameters on part performance due to fiber orientation.

Using finite element analysis to estimate fiber orientation has been well devel-

oped for traditional polymer composites and is integrated with the industry-leading injection molding simulation environment Moldflow<sup>®</sup>. The basis for this analysis is primarily the Folgar-Tucker model, developed as a process of modeling fiber orientation and how competing phenomena in injection molding affect it. This model has been rigorously tested and reinforced with experimental findings for traditional polymer composites but it is useful to study the utility of this model in new thermally-enhanced composites.

This paper presents a methodology for collecting and analyzing samples to determine fiber orientation in relatively large sections and develop both a qualitative and quantitative comparison to Moldflow<sup>®</sup> predictions. While this approach is not necessarily new, the goal of developing a more global understanding of fiber orientation in sample parts is generally counter to the recent progression of more precise and intricate measurement of fiber orientation that is not suitable for rapid testing and large test regions.

## 4.2 Background

With the introduction of fibers to polymer matrices, anisotropy can develop in the resulting material properties of the polymer composite. This is due to the directionality of the fiber's inherent properties, with much larger values along the length of the fiber compared to transverse to the length of the fiber. The orientation of the fibers within the polymer matrix therefore affects the benefits imparted to the polymer composite with a great improvement along the primary fiber direction

and minimal improvement along the transverse direction. This is demonstrated in Figure 4.2, with the greatest improvement in the loading response of the test sample occurring when the fibers are well aligned and the load is applied in the fiber direction. Applying the load in the transverse direction results in minimal improvement due to the introduction of fibers and when the fibers are evenly distributed in a random orientation an averaging effect occurs. [21, 64]

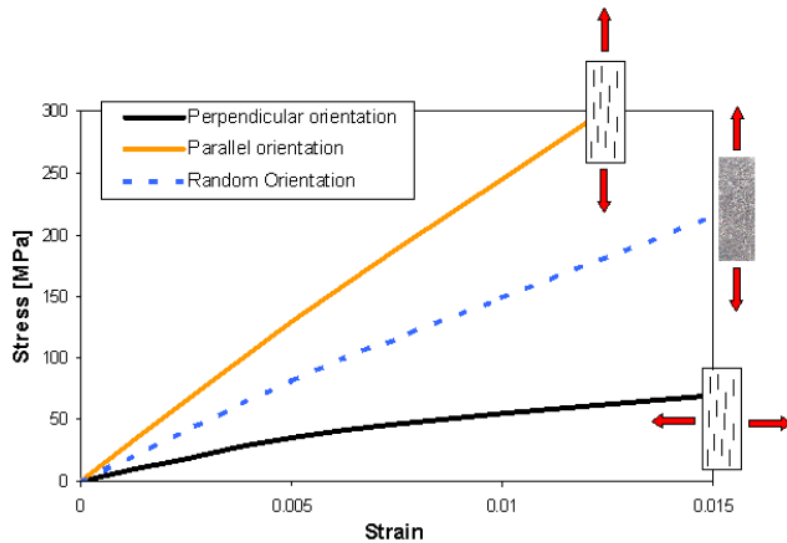


Figure 4.2: Stress-strain curve for varying fiber orientation and loading of a sample geometry. [21]

Similar to the structural example given above, fiber orientation affects the thermal conductivity of thermally-enhanced polymer composites. The thermal conductivity is greatest along the length of the fiber and it is therefore important to understand the fiber orientation in heat exchanger geometry to ensure that areas where heat transfer between mediums primarily occurs have the necessary fiber orientation to best accomplish this. While manufacturers advertise remarkable average

or maximum thermal conductivity values for thermally-enhanced polymer composites, the actual thermal performance could be dramatically affected by the fiber orientation within the heat exchanger. Therefore, it is important to understand and account for the fiber orientation within a component during the design stage in order to realize the full potential of fiber-filled polymer composites.

## 4.3 Related Work

### 4.3.1 Fiber Orientation

The Folgar-Tucker model for fiber orientation in concentrated suspensions, [29], provides the foundation for predicting fiber orientation in injection molding. This model uses parameters such as shear stress, viscosity, and velocity flow field to determine how fiber align as the injection molding process progresses. This model has been rigorously studied and is the accepted prediction method in industry-standard injection molding simulation tools such as Moldflow<sup>®</sup>.

This model, in its most frequently used form, utilizes tensors to provide a compact representation of fiber orientation [1]. Fundamentally, each fiber is represented as a vector,  $\mathbf{p}$ , with two angles,  $\theta$  and  $\phi$ , as shown in Figure 4.3. The vector components can be found using this representation with Equation 4.1, shown below.

$$\begin{aligned}
 p_1 &= \sin \theta \cos \phi \\
 p_2 &= \sin \theta \sin \phi \\
 p_3 &= \cos \theta
 \end{aligned}
 \tag{4.1}$$

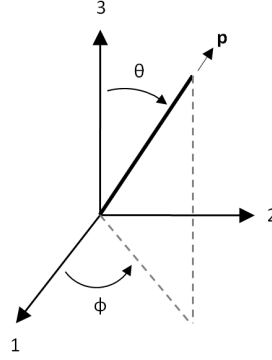


Figure 4.3: Vector representing fiber orientation.

With each fiber defined as a vector, the most common representation of fiber orientation is the probability distribution function for orientation,  $\psi$ . This distribution is then presented concisely as a second-order tensor using Equation 4.2 over all directions. The tensor value represents the overall orientation distribution of a sample region and Figure 4.4 demonstrates some example tensor values.

$$a_{ij} = \oint p_i p_j \psi(\mathbf{p}) d\mathbf{p} \quad (4.2)$$

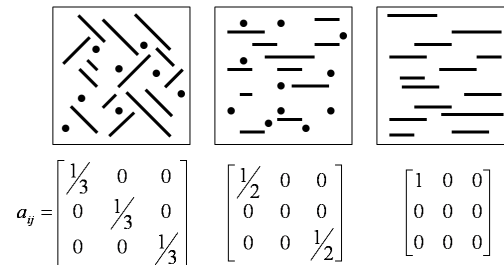


Figure 4.4: Example tensor values.

While some fiber measurement schemes use three-dimensional information to determine fiber orientation [62, 16], the majority of methods utilize imaging two-

dimensional cross-sections and determining fiber orientation from these sections. Using the fundamental geometry of fibers and the vector representation described previously, the fiber orientation of a given fiber can be determined based on the dimensions of the elliptical cross-section, shown in Figure 4.5, and is detailed in Section 4.5.4. While this method is very useful for determining fiber orientation from simple cross-sections, there exists ambiguity in determining the out-of-plane angle for a given cross-section, as shown in Figure 4.6. This affects values for two of the six tensor components,  $a_{13}$  and  $a_{23}$ , and should be taken into consideration when evaluating fiber orientation measurements.

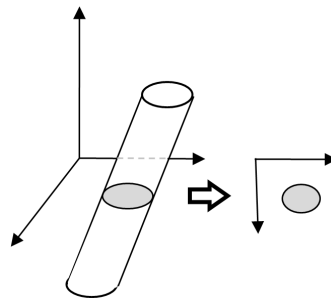


Figure 4.5: Fiber cross-section for determining orientation.

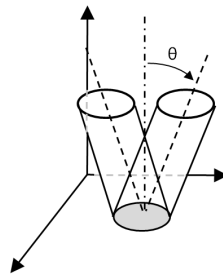


Figure 4.6: Issue resolving sign of out-of-plane angle using simple cross-section.

### 4.3.2 Experimental Methodologies

Much work has been done on developing methodologies for increasingly more accurate measurement of fiber orientation in test samples. There are three primary components of experimental measurement that have received significant attention: sectioning techniques, imaging methods, and image processing algorithms.

**Sectioning Techniques.** The development of sectioning techniques has progressed primarily with the goal of providing the most useful information for image processing. Initial methods used sectioning and polishing technologies from traditional experimental applications and used single sections of a region of interest to develop an understanding of the accuracy of fiber orientation predictions for the sample [28, 36]. The progression from this simple sectioning technique has generally been used to develop a more accurate three-dimensional representation of fiber orientation by using methods such as multiple slice sections or sections at multiple angles. Using multiple slices that are minimal thickness apart allows the direction of fibers to be tracked and used to accurately determine the out-of-plane orientation components [20, 52, 77]. While this method offers more precision with a fully-resolved 3D orientation, it is a more intensive process due to its requirements for aligning the results from the multiple sections through the use of complex registration schemes or other alignment methods. Using sections at multiple angles can provide significant information for determining fiber orientation and allows a much better understanding of how fiber orientation changes throughout the sample [8]. While this is valuable, preparing multiple sections introduces significant complex-

ity and labor into the experimental process and may limit the size of sections and therefore the useful area that can be studied.

**Imaging Methods.** With the sample geometry sectioned and polished for imaging, there are many options that have been explored for measuring fibers in a test section. The original and most common method is optical microscopy [8, 20, 77]. This method is attractive due to its high availability and lack of complexity for quickly implementing sampling methodologies but its primary drawback is that it is difficult to measure out-of-plane orientation components due to the strictly two-dimensional imaging behavior, although this has been resolved through the use of advanced sectioning methods. Other imaging methods that have been investigated include X-rays [42], Scanning electron microscopy [2, 61], and confocal microscopy [25]. X-ray imaging is potentially useful for nondestructive testing but often requires complex sectioning for useful results and may require substitution of materials that are readily X-ray compatible. Scanning electron microscopy provides a remarkably detailed image of fiber orientation and through advanced methods, such as Shadow SEM Analysis [61], out-of-plane orientation can be determined using a single section. Unfortunately the high magnification utilized in SEM analysis is not suitable for measuring fiber orientation over large sample sections. Confocal microscopy uses clever imaging techniques to extract three-dimensional orientation information from two-dimension images and is therefore useful for single sectioning methods but it lacks availability and may be too complex for general experimental usage.

**Image Processing Algorithms.** Initial image processing techniques often used manual fiber identification [8] for processing but more powerful computing

platforms and image processing techniques have dramatically advanced the process and led to significant automation. The ability to sample large areas was improved with the use of image analysis tools to align and order sequentially collected images and the ability to analyze fiber orientation in real time [20]. Recent work has led to intricate identification and visualization of the three-dimensional fiber orientation of test samples [62] and represents the advancing accuracy of fiber orientation measurement.

#### 4.4 Problem Definition

Based on the progress that has occurred in developing experimental methods for measuring fiber orientation, and the various advantages and limitations that are associated with them, along with the specific motivation for this project, the following goals were identified for developing the experimental methodology for this study:

1. **Low Magnification:** Use standard, relatively low-magnification, light microscopy to collect image samples due to its high availability and ability to sample large test sections.
2. **Single Sample Section:** Use a single section and standard polishing technique to prepare samples for imaging to ensure that the process can be applied to a large variety of materials and reduce the complexity of preparing samples.
3. **Use Goal Material:** Use the target material for the sample geometry in its

applied form rather than specially-designed materials with tracers or other unique fillers so that results represent the behavior of the final product.

4. **Control Tensor Region:** Provide granular control of the tensor calculation region size in order to provide both global and local representation of the fiber orientation across the sample geometry.
5. **Standardized Tools:** Use standardized image processing and tensor calculation techniques to take advantage of common understanding and build upon established methods.

## 4.5 Approach

The approach developed for this project is divided into two primary sections: the experimental setup for collecting fiber orientation information and the image processing framework for interpreting the found fiber orientation information. The presented approach presents the experimental procedure required to compare the fiber orientation information for a sample geometry to simulation predictions using both qualitative and quantitative methods.

### 4.5.1 Experimental Setup

**Sectioning.** Due to the destructive nature and labor intensity of sectioning samples, a single sample section methodology was chosen for this study. Therefore, careful consideration must be given to selecting a sample section that will provide the most useful information about the fiber orientation behavior in a sample geometry.

For methods where large areas can be sampled, the section that gives that largest sample region may be the best choice although any particular regions of interest should be accounted for. Traditionally, small test regions are selected to measure the fiber orientation in a particular location while large test regions can be used to analyze more complex behavior, such as how far from the injection location that fibers reach a certain level of alignment, and other properties that contribute to a more global understanding of the fiber orientation in a test part.

**Polishing.** After selecting a suitable test section, a grinding and polishing procedure is used to prepare the test sample. This procedure was developed following traditional best practices and designed to use standard polishing equipment. A polishing schedule was formulated based on the work of [35] and [63] to ensure a uniform, highly polished section for microscope imaging. Initial coarse grinding was used to approach the desired section dimensions and flatten the surface with some thickness remaining to be removed in subsequent polishing steps, ensuring the desired thickness is met after sufficient polishing. Using a polishing wheel with water lubricant, gradually finer grit sizes are used for rough polishing while constantly moving and rotating the test specimen to eliminate any directional markings or striations that could be introduced due to the circular motion of the polishing wheel and thoroughly cleaning the specimen between steps to remove any contaminants. The polishing procedure is completed with fine polishing using diamond paste and a water lubricant. This procedure was found to consistently produce well-polished specimens suitable for light microscopy.

**Microscope Imaging.** The microscope chosen for this approach was a tradi-

tional light microscope with polarizing filter technology. Reflected light was chosen to alleviate the need for thin slices that are required for transmitted light. The polarizing filters were used to take advantage of the differing characteristics of the fibers and the surrounding matrix material, and were adjusted to reinforce the reflected light from the fibers and light absorbed in the polymer matrix. This method was shown to produce high contrast for carbon fiber filled polymer composites and should be useful for most fiber-filled polymers with significant differences between the fiber and matrix materials. A relatively low magnification of 5x was chosen to provide a clear picture of the fibers in the matrix while providing a wide enough view in order to sample large sections.

#### 4.5.2 Fiber Orientation Comparison Framework

A fiber orientation comparison framework was developed to take large sample sections consisting of many microscope images, analyze and determine fiber orientation for the entire sample, and then compare these results with simulation predictions. Details of this process include the goal of controlling the examined size for making fiber orientation measurements and developing both a local and global understanding of fiber orientation for comparison to predicted values. This framework progresses as a six-step process and is presented below.

**Step 1. Initialization.** The initialization stage is primarily used to define the connection to microscope images and customize image processing settings for the particular application. It is also used to define the relationships between the

microscope images and how they correspond to the overall test section to ensure the individual results properly correlate to the overall behavior.

**Step 2. Perform Image Processing on Original Images.** Image processing, detailed in Section 4.5.3, is applied to all of the original microscope images to extract raw orientation information for all of the fibers found in each image.

**Step 3. Combine Image Results and Subdivide into Tensor Regions.** With the raw fiber orientation information found for each image, the results are combined to form the overall sample section. This includes cropping original images to remove any overlap or other requirements for resizing and arranging results information to properly correspond with positioning in the test section.

With the sample section reconstructed from its component images, it is then subdivided into regions for tensor analysis. This method was chosen instead of using the original image regions to calculate tensor values in order to provide more control of the tensor region size. This control over the resolution of measured tensor values allows better comparison to predicted values due to the ability to find both local and global information using high-resolution and low-resolution tensor regions, respectively. It can also be used for measurement quality control such as ensuring there is sufficient fiber information in a selected tensor region for accurately determining tensor values.

**Step 4. Calculate Tensor Values.** Using the defined tensor regions, tensor values are calculated to represent fiber orientation, described in Section 4.5.4.

**Step 5. Subdivide Simulation Results and Sample Tensor Values.** Using the same defined tensor regions as the experimental results, subdivide the

simulation results. The tensor values are then sampled in these tensor regions to determine the tensor values corresponding to the found experimental values. The simulation results present the tensor components as a continuous value across the tensor region so a representative tensor value is found by sampling multiple points within the tensor region and determining the average tensor value for each region to compare with the measured experimental values.

**Step 6. Compare Experimental and Simulation Tensor Values.** With both measured experimental tensor values and predicted tensor values, the fiber orientation information is compared across the sample section, shown in Section 4.5.5.

### 4.5.3 Image Processing Algorithm

The image processing algorithm was developed using open-source tools (OpenCV) and standard techniques to build upon a common and well-developed foundation for the image processing framework and allow wide availability for potential applications. Additionally, the algorithm was designed to be flexible to changing sample materials that can lead to varying contrast between fiber and matrix materials, fiber size, and other properties to ensure that the goal materials for varying applications can be used. The steps below outline the major stages of the develop image processing algorithm.

**Step 1. Resizing, Down Sampling, and Smoothing.** This step is used to define a common set of input image parameters and prepare the raw microscope image for processing. The image resizing and down sampling (performed via Gaussian

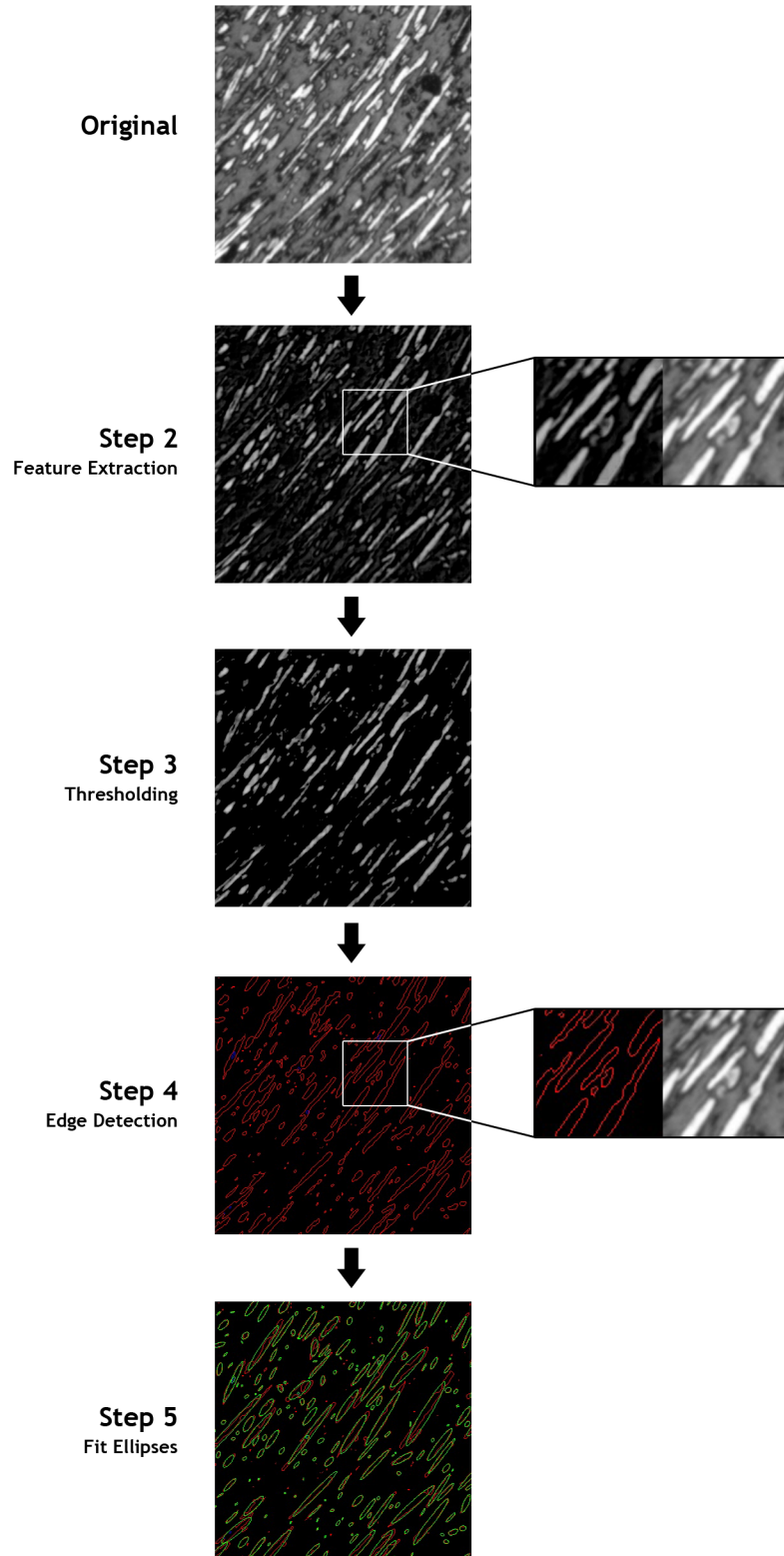


Figure 4.7: Progression of image processing algorithm for identifying fibers, described in Section 4.5.3.

Pyramidal decomposition) are used to ensure that the measured fibers are within a defined general size for consistent processing in subsequent steps. The smoothing is performed to remove noise that can be introduced from the microscope and camera system.

**Step 2. Feature Extraction.** To better differentiate between fibers and the surrounding matrix material, feature extraction is performed on the prepared microscope image. This process, developed in the field of mathematical morphology and known as a top-hat transformation, uses a defined structuring element to explore the image to find areas that the structuring element fits into that are brighter than their surroundings. The structuring element is sized so that it is smaller than the general fiber size and isolates the fibers from the dark matrix background.

**Step 3. Thresholding.** With the fibers well defined from the background material, a thresholding operation is applied to separate the image into light areas representing fibers and dark areas representing the matrix material. After the thresholding application is complete, the areas of the image that contains fibers have a value of 1 and all other areas are 0, allowing for more precise application of image processing techniques in the following steps.

**Step 4. Edge and Shape Detection.** Edge detection is then applied to identify all of the transition regions between fiber and matrix values. Shape detection is then used to locate continuous edges, saving each contour as a sequence of points.

**Step 5. Fit Ellipses to Detected Shapes.** Finally, each contour is processed and if it has greater than six points a two-dimensional box is fit such that it is the minimal size containing the contour and is represented by an ellipse for

the processed image. Each ellipse denotes a fiber found in the processed image and its geometrical properties are saved for use in calculating the fiber orientation information for the sample.

Using the developed image processing algorithm, the supplied microscope image is analyzed and each fiber is isolated and marked with an ellipse. This set of ellipses representing the found fibers is the output of the algorithm and contains the geometric information necessary for calculating fiber orientation tensor values for the measured area.

#### 4.5.4 Tensor Calculation

With the set of ellipses representing the found fibers from the image processing analysis, the fiber orientation tensors for a defined region can be calculated. Using the ellipse formulation shown in Figure 4.8, the required ellipse properties, such as minor and major axis length ( $m$  and  $M$ , respectively), can be calculated using Equations 4.3-4.5.

$$m = \sqrt{(x_3 - x_4)^2 + (y_3 - y_4)^2} \quad (4.3)$$

$$X = x_2 - x_1, Y = y_2 - y_1 \quad (4.4)$$

$$M = \sqrt{X^2 + Y^2} \quad (4.5)$$

With each fiber fully defined as an ellipse, the tensor values can be calculated for the fibers contained within a specified region using Equations 4.6 and 4.7 and Table 4.1. In Equation 4.6,  $a_{ij}$  represents the overall tensor component for the region, and  $(a_{ij})_n$  represents the tensor component for the  $n$ th fiber (shown in Table 4.1).

$F_n$  is a weighting function used to cope with the biasing that can occur due to fibers lying predominantly perpendicular to the sample section being more likely to appear in the specified region.

$$a_{ij} = \frac{\sum (a_{ij})_n F_n}{\sum F_n} \quad (4.6)$$

$$F_n = \frac{M_n}{m_n} \quad (4.7)$$

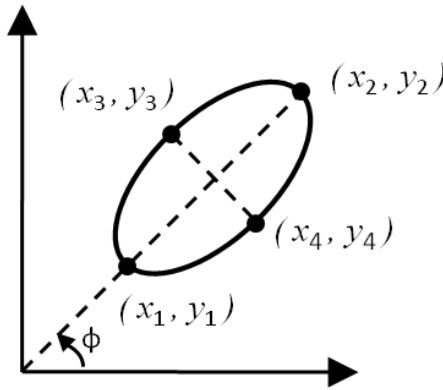


Figure 4.8: Elliptical fiber cross-section for determining orientation.

#### 4.5.5 Comparing Experimental and Simulation Results

While the fiber orientation for the experimental sample is useful by itself, for the purpose of this study it is most valuable and informative when compared to predicted values in order to refine the prediction methodology to more accurately represent actual behavior. There are four primary aspects that were considered when developing the comparison approach: quantitative and qualitative comparison and local and global understanding. The varying tensor calculation region, discussed

Table 4.1: Tensor components for a single fiber.

Tensor component for $n$ th fiber	Representation with measured geometrical parameters
$(a_{11})_n$	$X^2 \left( \frac{1}{M^2} - \frac{m^2}{M^4} \right)$
$(a_{12})_n = (a_{21})_n$	$XY \left( \frac{1}{M^2} - \frac{m^2}{M^4} \right)$
$(a_{13})_n = (a_{31})_n$	$X \sqrt{\frac{m^2}{M^4} - \frac{m^4}{M^6}}$
$(a_{22})_n$	$Y^2 \left( \frac{1}{M^2} - \frac{m^2}{M^4} \right)$
$(a_{23})_n = (a_{32})_n$	$Y \sqrt{\frac{m^2}{M^4} - \frac{m^4}{M^6}}$
$(a_{33})_n$	$\frac{m^2}{M^2}$

previously in Section 4.5.2, provides the foundation for determining the overall local or global representation of the results but the quantitative versus qualitative understanding is more dependent on how the results are presented.

**Quantitative and Qualitative Comparison.** By measuring fiber orientation information for both experimental and predicted samples, a wide variety of both quantitative and qualitative comparisons can be made. Examples of qualitative comparisons include determining geometry changes that lead to divergence between predicted and actual fiber orientation, understanding how long after geometry changes it takes fibers to reach reasonable alignment, discovering limits for processing conditions at which prediction performance diminishes. When fiber orientation tensor values are known, quantitative values can be determined or assigned for each of these qualitative comparisons and have potential uses such as calculating the ratio between the change in angle for a geometry and the rate of prediction

divergence, measuring the distance to reasonable alignment from a point of interest, or determining bias values based on processing conditions. Therefore, having measured fiber orientation values across a large sample region allows for powerful quantitative and qualitative comparisons that can be useful for designers and in the development of tools to integrate experimental studies with simulations for more accurate and useful predictions.

**Local and Global Understanding.** By designing the image processing framework to locate fibers even at low magnification, much larger sample cross-sections can be used to form a much more global representation of fiber orientation over complicated geometries. Recent work with fiber orientation has trended towards much more precise understanding of fiber orientation using very high magnification sources such as SEM. While this is very useful for understanding how to improve fiber orientation prediction and are invaluable to improving simulation predictions, this has a very limited understanding of the overall fiber orientation behavior in sample geometries. This study makes use of relatively low-magnification imaging and widely-used image processing software to create a more global perspective of the fiber orientation in sample geometries. While these techniques do not necessarily have the same accuracy as high-magnification methods, the loss in accuracy is made up for by having a much more complete understanding of the overall fiber orientation behavior and how it potentially affects simulation predictions, processing decisions, and design choices.

#### 4.5.6 Problem Formulation Details

**Test Geometry.** An L-channel shape was chosen due to the highly uncertain behavior that occurs in the corner region and its prevalence in component design and specifically heat exchanger design. This geometry is useful for understanding how processing conditions and geometric properties can affect fiber orientation behavior in a drastic flow change and determining more complex phenomena such as how far from the corner it takes for the fiber orientation behavior to settle to a more consistent and well-aligned situation. This test geometry along with part of the injection mold used to create it are shown in Figure 4.9.

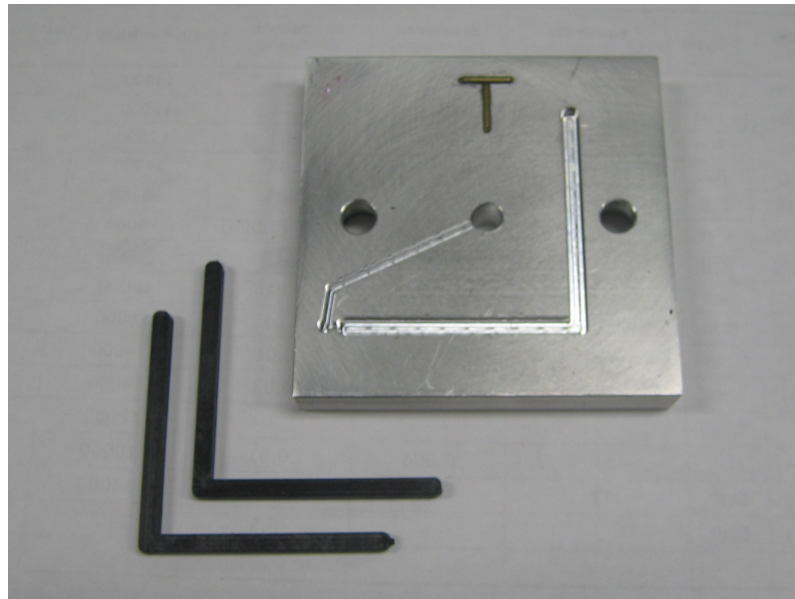


Figure 4.9: L-Channel mold with parts.

**Test Material.** In order to most accurately reflect the behavior of the proposed heat exchanger design, the material selected for the proposed design was used for this test geometry. This material is a commercially-available carbon-fiber filled

Nylon 12, PolyOne NJ-6000 TC Black. The manufacturer-recommended injection molding processing conditions along with the injection molding machine specifications were used to determine the processing conditions for manufacturing the test samples, detailed in Table 4.2.

Table 4.2: Processing conditions for test sample.

<b>Processing Condition</b>	<b>Value</b>	<b>Units</b>
Injection Pressure	164	MPa
Injection Flow Rate	12	cm <sup>3</sup> /s
Melt Temperature	285	°C
Mold Temperature	30	°C

**Experimental Procedure Details.** The cross-section at the [midplane of the longest direction], demonstrated in Figure 4.10, was chosen because it provided the most information on the overall fiber orientation of the geometry in a single cross-section, a goal of the developed approach. A polishing apparatus, shown in Figure 4.11, was constructed to provide a precise polishing base and improve surface uniformity and quality. The polishing routine described in Section 4.5.1 was used with the details shown in Table 4.3a below.

With the sample sectioned and polished, it was microscope imaged to collect raw fiber orientation information. Based on an exploratory analysis, Table 4.3b provides the microscope setup that supplied the most contrast between the fibers and surrounding matrix, with the fibers reflecting the supplied light and appearing white in the collected images and the matrix absorbing the supplied light and appearing black. Based on this procedure, Figure 4.12 demonstrates a microscope

image collected for the test section.

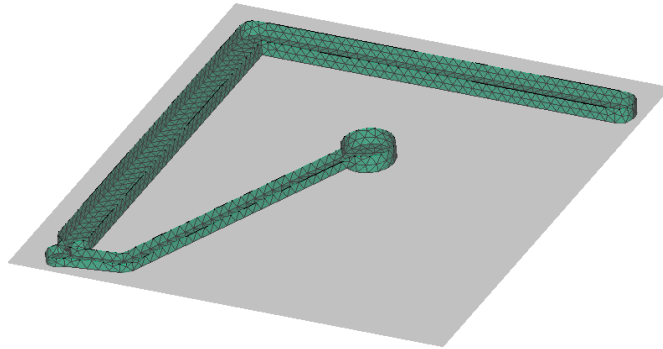


Figure 4.10: Sectioning plane for test geometry.

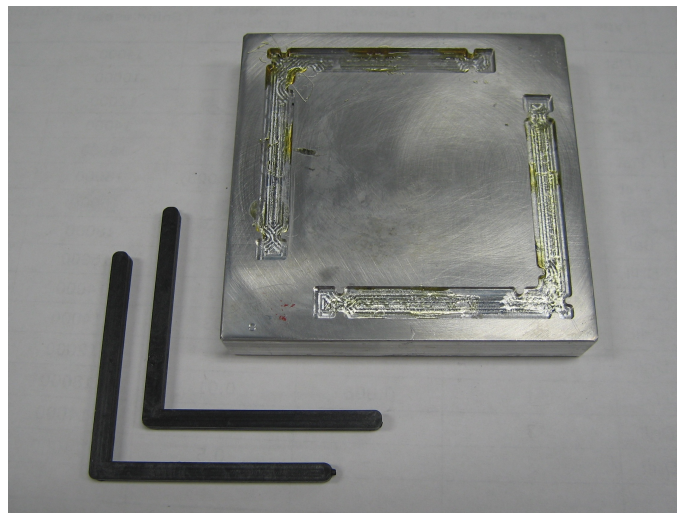


Figure 4.11: L-Channel polishing jig.

## 4.6 Results and Discussion

**Validation Image.** To validate the image processing and tensor calculation framework, the sample image shown in Figure 4.13 was used. This image was used

Table 4.3: Experimental procedure details.

(a) Polishing schedule used to prepare test samples.

Step	Details	Time
1. Initial Dressing	240-400 Grit, water lubricant	As Needed
2. Fine Grinding	800 Grit, water lubricant	5 min
3. Rough Polishing, 1	1200 Grit, water lubricant	5 min
4. Rough Polishing, 2	3.5 $\mu$ m, water lubricant	5 min
5. Fine Polishing, 1	6.5 $\mu$ m diamond paste, water lubricant	30 min
6. Fine Polishing, 2	1 $\mu$ m diamond paste, water lubricant	30 min

Each step is performed with light pressure while constantly moving the specimen and followed by thorough cleaning, drying, and examination

(b) Selected microscope settings.

Parameter	Value
Light Source	Reflected
Magnification	5x
Polarizer 1	0°
Polarizer 2	60°

by [8] to test measurement error and the exact tensor values are given. These values and the corresponding calculated values are shown in Table 4.4 and demonstrate excellent agreement. The small error in the calculated values can be attributed to a range of factors, such as the scanning process used to create the image, but is negligible and therefore the developed image processing and tensor calculation framework has sufficient accuracy for experimental studies.

**Simulation Framework.** Using the processing conditions outlined in Table 4.2, Moldflow<sup>®</sup>, the industry-standard injection molding simulation tool, was used to predict fiber orientation in the sample L-channel geometry. The fiber ori-

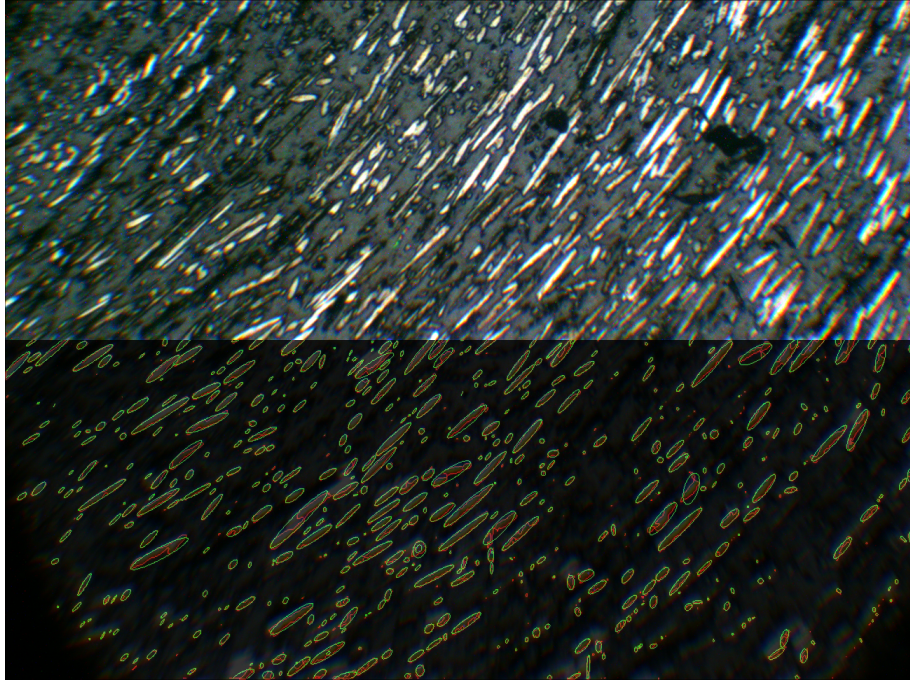


Figure 4.12: Example of collected microscope image with image processing results overlaid on lower half.

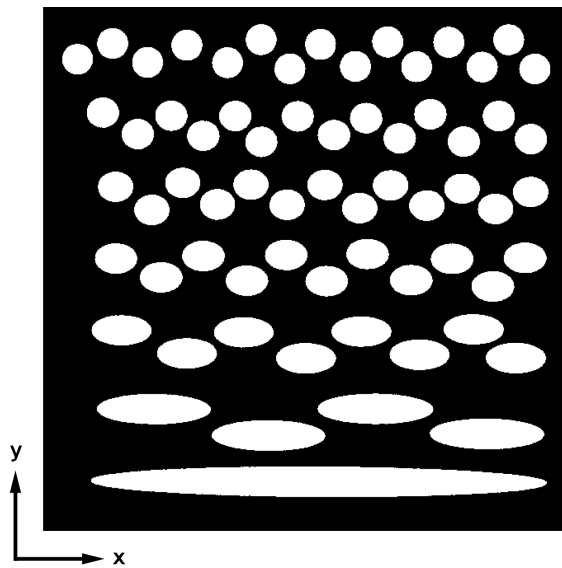


Figure 4.13: Measurement validation image.

Table 4.4: Exact and calculated tensor values for the measurement validation image.

<b>Tensor Component</b>	<b>Exact Value</b>	<b>Calculated Value</b>
$t_{xx}$	0.5087	0.5003
$t_{yy}$	0	0.0011
$t_{zz}$	0.4913	0.4987
$t_{xy}$	0	0.0004

entation analysis component of Moldflow<sup>®</sup> presents the results as either the three principle tensor values or the six tensor components in the global coordinate frame. The principle tensor values are a representation of the fiber orientation tensor in a special coordinate system in which the shear tensor components ( $t_{xy}$ ,  $t_{xz}$ , and  $t_{yz}$ ) are zero and is useful for gaining an understanding of the magnitude of the primary tensor components with respect to the polymer flow. For this study, the calculated tensor components are determined with respect to the global coordinate frame and therefore the primary tensor values can not be used and rather the full tensor component representation must be used.

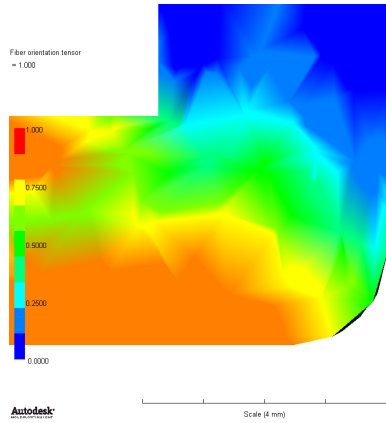
Figure 4.14 shows the tensor components in the corner region of the L-channel geometry in which the polymer flow experiences a significant velocity change and subsequently a high level of uncertainty exists in the predicted fiber orientation values. The tensor components are calculated at each node in the meshed model and then a process of multi-linear interpolation is used to create a continuous representation of the tensor components across the test geometry. This is useful for the comparison framework because the tensor values can be determined for any tensor

region size and position.

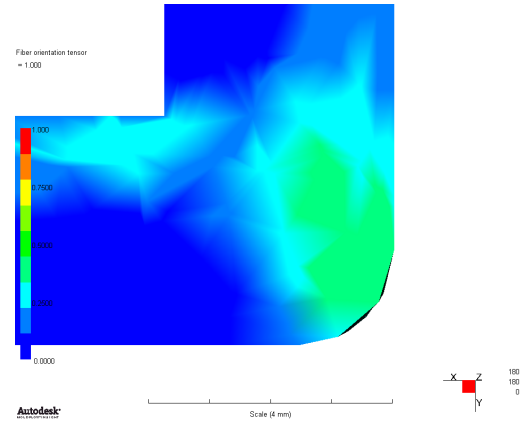
**Comparison Results.** The L-channel was sampled at 5x magnification and analyzed across the shown region. A sample image with the processed results is shown below. The image processing framework was effective in identifying most of the fibers in the sample images and was used to successfully develop tensor plots for comparison to Moldflow<sup>®</sup> results.

First, a more global understanding of the fiber orientation behavior in the corner region of the L-channel was investigated. Figure 4.15 shows the comparison of the Moldflow<sup>®</sup> predictions and the experimental measurements with a relatively coarse tensor region size, where the flow enters from the top of the corner and exits to the left. The primary tensor components,  $t_{xx}$ ,  $t_{yy}$ ,  $t_{zz}$ , and  $t_{xy}$ , are shown since they show most of the behavior and due to the inability to resolve the signs for the remaining out-of-plane components.

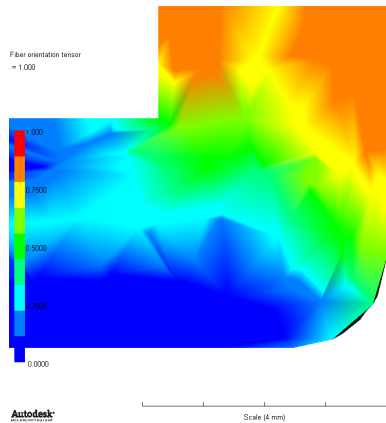
It is shown that throughout the sample, the level of correlation varies greatly. There are regions which the predicted and experimental values match closely and others which the values diverge greatly. Although this result is significant, it should not be assumed that either the Moldflow<sup>®</sup> prediction is incorrect or the measurement is invalid. The L-channel geometry was chosen specifically due to the very high uncertainty that occurs in the sharp velocity change and the difficulty that arises in simulating this behavior. Therefore, these findings do not suggest that there are underlying flaws in the employed Moldflow<sup>®</sup> fiber orientation models, just limitations in highly uncertain flow situations for which predictions may be insufficient and measured values should be used instead.



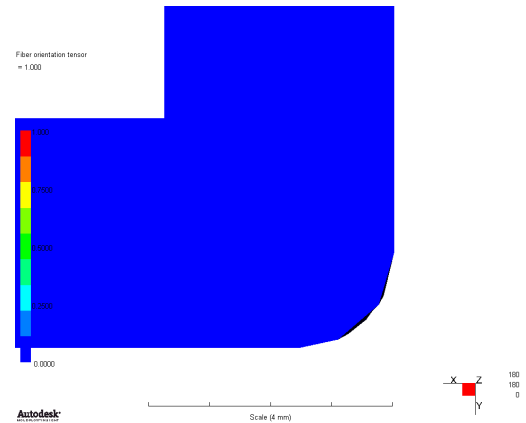
(a)  $t_{xx}$ .



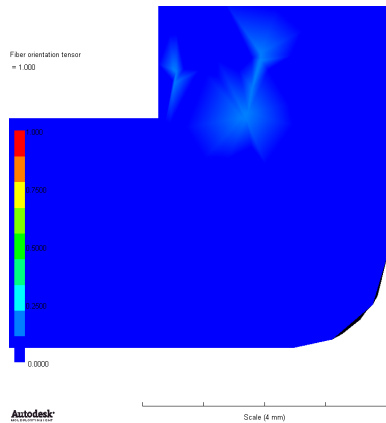
(b)  $t_{xy}$ .



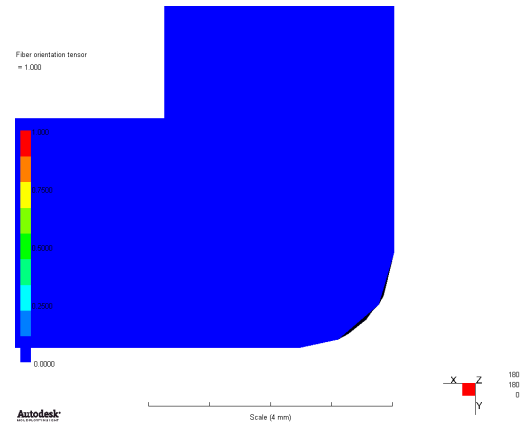
(c)  $t_{yy}$ .



(d)  $t_{xz}$ .



(e)  $t_{zz}$ .



(f)  $t_{yz}$ .

Figure 4.14: Moldflow<sup>®</sup> tensor component results.

The primary out-of-plane fiber orientation tensor component,  $t_{zz}$ , is negligible in the Moldflow<sup>®</sup> predictions but not in the experimental findings. This signifies an important design improvement in the out-of-plane thermal performance and could lead to improved application results compared to the simulation predictions. The conservative fiber orientation models did not predict out-of-plane orientation for the in-plane velocity change and therefore design changes that could have been introduced to improve out-of-plane alignment would not have registered in simulation predictions. This represents the importance of incorporating experimental fiber orientation measurements during the design phase to ensure the heat exchanger that best utilizes fiber orientation can be created.

Next, the exit region of the test sample was investigated locally using a high-resolution tensor region, shown in Figure 4.16. This investigation allows for a more quantitative comparison of the Moldflow<sup>®</sup> predictions and experimental values. Again, differences between predicted and measured values should not be used to disregard either value. Instead, experimental findings can be used to bias or refine predictions in certain geometries and other instances in which it is found that they diverge.

Based on the findings shown in Figure 4.16, the following general conclusions can be drawn for this example. First, insufficient fiber information was collected along the left edge of the region to determine tensor components for the left-most tensor regions. The primary out-of-plane tensor component,  $t_{zz}$ , shows little variation across the section but the simulation predictions are too conservative in assuming no out-of-plane alignment and there is poor agreement with the measured

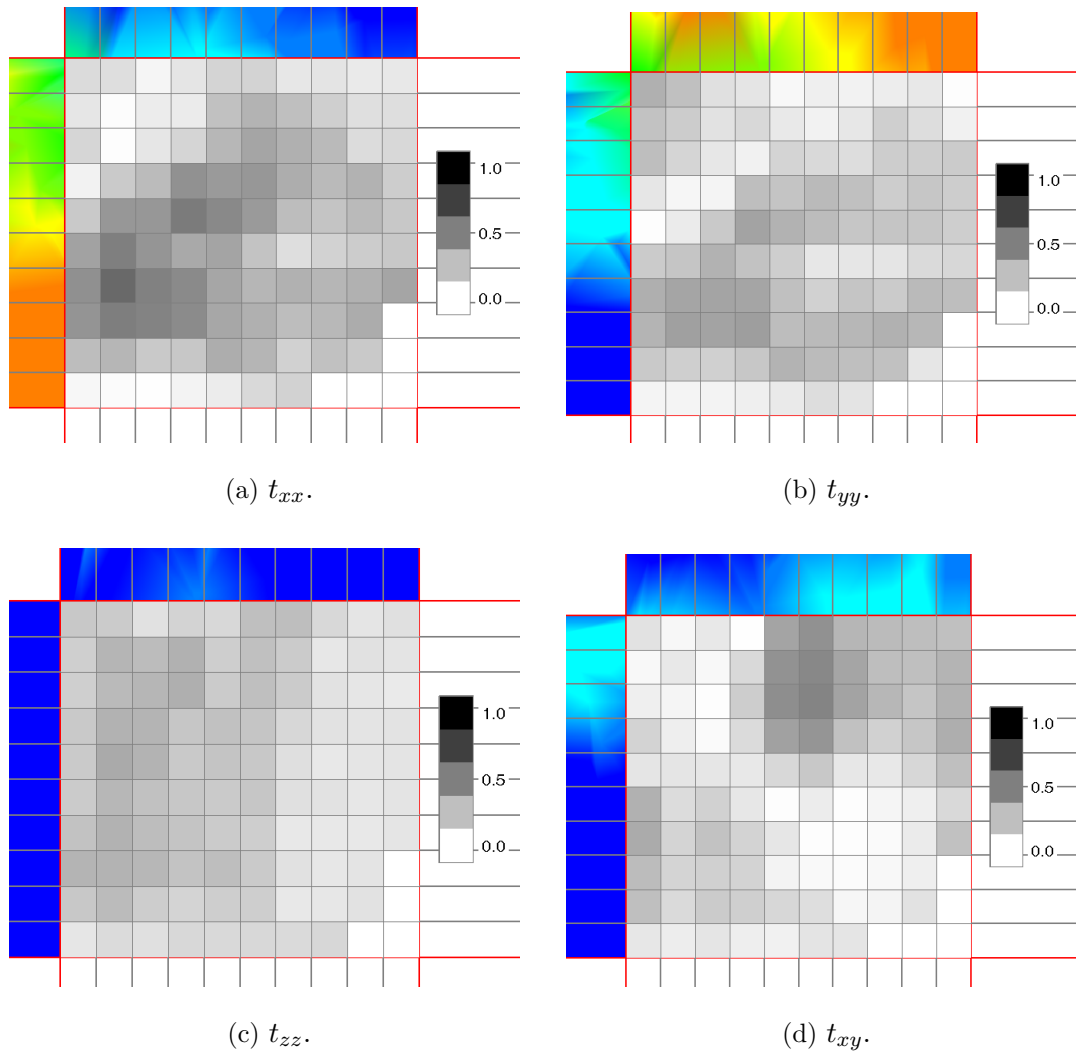


Figure 4.15: Tensor results.

values.  $t_{xx}$  and  $t_{yy}$  correspond most directly with the direction of flow for the polymer and show poor agreement in the central region at the exit of the corner while the surface areas at the inside and outside of the corner have strong agreement between predicted and measured values. This indicates a high level of uncertainty at locations away from the mold walls and generally increasing uncertainty with increasing

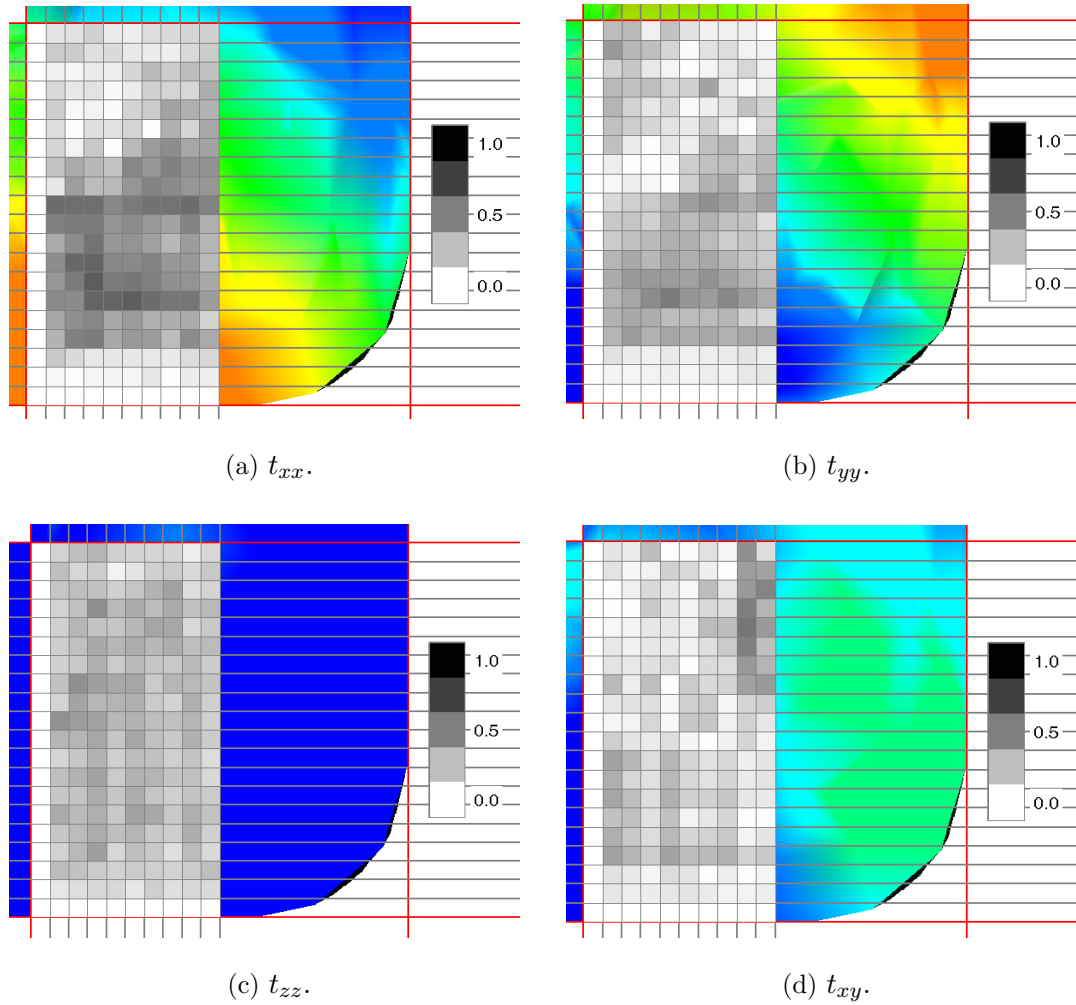


Figure 4.16: Detailed tensor results.

radius from the interior of the corner. For this example, it would be valuable to use experimentally measured values for centrally located regions in geometries with rapid velocity changes while predicted values should be sufficient for the remainder of the test region.

## 4.7 Summary

Thermally-enhanced and other fiber-filled composites that have been introduced into the polymer marketplace can lead to dramatic improvements in material properties, including thermal conductivity and structural factors, but these properties are affected by the fiber orientation within the component. Finite Element Analysis techniques have been applied to predict fiber orientation in injection-molded components, but these methods were developed for more traditional fiber-filled composites and the improved thermal conductivity and high volume concentration in thermally-enhanced composites require additional verification of fiber orientation predictions. This chapter presents an approach to experimentally measure and calculate the fiber orientation information for sample parts and demonstrates a comparison framework for comparing measured values to fiber orientation values predicted by the industry-standard injection molding simulation tool Moldflow<sup>®</sup>.

Previous work in experimentally determining fiber orientation was found to have three primary focuses when developing experimental methodologies: sectioning techniques, imaging methods, and image processing algorithms. Recent work in studying fiber orientation has trended to developing a more accurate measurement of fiber orientation using higher resolution imaging, complex sectioning, and advanced image processing techniques. While this has led to many advancements in the field of polymer composites, these techniques may be too complex to implement for large test regions and in general frameworks for varying materials and geometries. The experimental methodology investigated in this paper has five goals:

low magnification using traditional light microscopy, utilize a single sample section, use actual material, control over the tensor region size, and the use of standardized image processing tools. The developed method successfully measured fibers in a simple section using traditional light microscopy and relatively low magnification and calculated fiber orientation tensor values at both high and low resolution for both a global and local understanding of fiber orientation. This allows the method to be applied to a range of fiber orientation measurement applications and reduces many barriers to implementation in many environments.

The developed approach was applied to studying an L-channel geometry representing a dramatic velocity change and representative of a behavior common among heat exchanger designs. A study of the corner region of this geometry found significant variance in the agreement between the predicted and measured values. The out-of-plane tensor values demonstrated consistent under-prediction in simulations with consistent measured out-of-plane alignment while the in-plane values varied from good agreement at regions near mold walls and poor agreement in central regions of the geometry. The high uncertainty in the corner region leads to a recommendation of using experimental values of fiber orientation in centrally located regions with dramatic velocity changes.

This study successfully developed a fiber orientation measurement framework for comparing experimental results to simulation predictions. This is useful for studying advanced materials for which the applicability of more traditional prediction tools is unknown. Additionally, the flexibility of the developed method allowed large sections to be studied while determining fiber orientation at granular levels to

develop both a global and local understanding of fiber orientation in the test sample. The tool uses traditional tools and open source methods to maintain availability for broad audiences. The developed method is useful for overall testing, such as manufacturing verification of expected overall fiber orientation in sample parts and is useful for determining a qualitative understanding of the fiber orientation behavior as well as generating qualitative results for direct comparison to simulation results.

## Chapter 5

### Conclusion

#### 5.1 Intellectual Contributions

The contributions of this work can be separated into three primary categories:

1. An approach for developing a computationally-fast metamodel that accurately predicts the feasibility boundary while requiring minimal sample datapoints has been presented and applied to create a mold filling metamodel for thermally-enhanced polymer composite plate-fin heat exchangers. This approach, the Feasibility Boundary Search algorithm, uses advanced Design of Experiments and adaptive control techniques to selectively sample points very close to the feasibility boundary across the entire design space to create a model that is highly accurate and applicable over a large range of design criteria. The developed metamodel, in addition to providing the injection molding feasibility of a candidate heat exchanger design, also predicts the minimum attainable base thickness for use in optimizing the heat exchanger design for thermal performance considerations.
2. A model simplification framework has been presented for providing an estimate of mold filling for general finned-plate geometries. This framework determines an equivalent flat plate representation of the given geometry and uses

a metamodel developed to provide an estimate of mold filling for flat plate geometries to predict mold filling for the original geometry. This approach dramatically reduces prediction time for finned-plate geometries by removing the need for computationally-intensive injection molding simulation and allows greater flexibility for any changes in the overall heat exchanger geometry.

3. A fiber orientation experimental measurement methodology has been presented for collecting fiber orientation information from sample geometry and comparing these findings with simulation predictions. This methodology details all of the necessary steps in the process, including preparing the sample for imaging, collecting microscope images, performing image processing to measure fiber orientation information, and calculating fiber orientation values. This approach was applied for a sample heat exchanger geometry to determine conditions for which injection molding simulation may be insufficient.

## 5.2 Anticipated Benefits

The work presented in this thesis provides an understanding of the manufacturability of thermally-enhanced polymer composites that is useful for designers of heat exchangers and many other applications. Most critically for the overarching goals of the polymer heat exchanger project, this work will be useful in developing a manufacturability component of a design exploration and optimization framework which considers thermal, structural, and manufacturing properties for the design of thermally-enhanced polymer heat exchangers.

In addition to the specific application for thermally-enhanced polymer heat exchangers, the frameworks presented in this thesis are useful for more general applications. The feasibility boundary metamodeling approach described in Chapter 2 is useful for any applications where developing a computationally-fast and accurate metamodel for determining feasibility considerations is required, such as structural analysis where failure modes are diagnosed via time-consuming physical experiments to determine feasibility. The experimental methodology presented in Chapter 4 is useful for many fiber orientation measurement applications and is particularly useful due to its ability to draw conclusions by comparing measured values to expected performance and its high-throughput analysis due to its simple sectioning and low magnification approach.

### 5.3 Future Work

While this thesis has significantly advanced the understanding of the manufacturability of thermally-enhanced polymer composites in heat exchanger applications, there are many areas in which future work can offer further insight. The main areas of interest for future improvement are directly related to the work that has been complete in this thesis.

#### 5.3.1 Improvement to Feasibility Boundary Search Algorithm

The Feasibility Boundary Search algorithm presented in Chapter 2 is a significant advancement in the development of metamodels representing feasibility for a

variety of applications. This approach used advanced Design of Experiments and adaptive control techniques but could be improved with additional refinements in the search algorithm. Some examples of how this approach can be improved include the use of an adaptive grid in place of the fixed grid size that was used for the design variables. This would ensure that areas of interest would have sufficient information collected while not collecting redundant or insignificant in other areas and could potentially lead to fewer datapoints being collected while maintaining or improving the accuracy of the developed metamodel. Additionally, the search behavior for finding points on the feasibility boundary could be improved with the use of machine learning and biasing techniques that could reduce the number of datapoints collected and ensure that each datapoint provides valuable information for the search algorithm. These improvements could reduce the computational intensity and improve the accuracy for developing feasibility metamodels.

### 5.3.2 Advancements in Model Simplification Approach

The model simplification approach presented in this thesis is a significant step towards developing a flexible mold filling prediction strategy for general finned-plate geometries. Potential improvements include developing a more robust prediction strategy for estimating the mold filling behavior based on geometric properties such as a weighted average fin height or the radius of gyration, representing fin spread. Additionally, the approach could be split by fin concentration to develop a separate model as concentration increases, alleviating the loss of accuracy as fin concentration

increased that was noted in the findings of this thesis. These advancements would expand the usability of this model simplification approach and make it more flexible for usage in a wide variety of applications.

### 5.3.3 Refinements for Fiber Orientation Measurement Methodology

The presented fiber orientation measurement methodology was designed to use simple sectioning techniques and low-magnification imaging to develop a more global understanding of the fiber orientation behavior in sample geometries. The microscope imaging could be made more accurate and consistent with the use of a computer-controlled stage and automatic capturing and alignment of microscope images. The image processing method could be improved to more accurately identify fibers and reduce discrepancies that arise due to behavior such as overlapping fibers or polishing defects. Finally the comparison framework can be improved to provide more useful information to designers on the actual fiber orientation behavior and integrated in a knowledge database or similar application to develop a more standardized approach to integrating experimental measurements during the component design phase.

## Bibliography

- [1] S. G. Advani and C. L. Tucker III. The use of tensors to describe and predict fiber orientation in short fiber composites. *J. of Rheology*, 31:751–784, 1987.
- [2] M. Akay and D. Barkley. Fibre orientation and mechanical behavior in reinforced thermoplastic injection mouldings. *J. of Materials Science*, 26:2731–2742, 1991.
- [3] C. Andújar, P. Brunet, and D. Ayala. Topology reducing surface simplification using discrete solid representation. *ACM Transactions on Graphics*, 4:133–144, 2002.
- [4] D. Attali, J. D. Boissonnat, and H. Edelsbrunner. Stability and computation of the medial axis—a state-of-the-art report. In *Mathematical foundations of scientific visualization, computer graphics, and massive data exploration*, 2004.
- [5] R. Bahadur. *Characterization, Modeling, and Optimization of Polymer Composite Pin Fins*. PhD thesis, Mechanical Engineering Department, University of Maryland, College Park, MD, 2005.
- [6] R. Bahadur and A. Bar-Cohen. Thermal performance limits of polymer composite pin fin heat sinks. In *Proceedings of the 55th Electronic Components and Technology Conference*, volume 2, pages 1720–1727, 2005.
- [7] A. Bar-Cohen, P. Rodgers, and J. Cevallos. Application of thermally enhanced thermoplastics to seawater-cooled liquid-liquid heat exchangers. In *Proceedings 5th European Thermal-Sciences Conference*, 2008.
- [8] R. S. Bay and C. L. Tucker III. Stereological measurement and error estimates for three-dimensional fiber orientation. *Polymer Engineering and Science*, 32, 1992.
- [9] J. P. Beaumont. *Runner and Gating Design Handbook: Tools for Successful Injection Molding*. Hanser Gardner Publications, 2004.
- [10] J. P. Beaumont, R. Nagel, and R. Sherman. *Successful Injection Molding: Process, Design, and Simulation*. Hanser Gardner Publications, first edition, 2002.
- [11] W. Bejgerowski, H. A. Bruck, and S. K. Gupta. A modeling approach for simulating heat dissipation from actuators and electronic components embedded in thermally conducting polymers. In *Proceedings of the ASME Computers and Information in Engineering Conference*, San Diego, CA, 2009.

- [12] W. Bejgerowski, S. K. Gupta, and H. A. Bruck. Multifunctional highly-filled polymer composites for embedding electronic components. In *Proceedings of the SEM Annual Conference & Exposition on Experimental and Applied Mechanics*, volume 1, page 85, Albuquerque, NM, 2009.
- [13] W. Bejgerowski, S. K. Gupta, and H. A. Bruck. A systematic approach for designing multifunctional thermally conducting polymer structures with embedded actuators. *J. of Mechanical Design*, 131(11):111009, 2009.
- [14] C. J. C. Burges. A tutorial on support vector machines for pattern recognition. *Data Mining and Knowledge Discovery*, 2:121–167, 1998.
- [15] J. Cevallos, S. K. Gupta, and A. Bar-Cohen. Incorporating moldability considerations during the design of polymer heat exchangers. *J. of Mechanical Design*, 2011. (accepted for publication).
- [16] A. R. Clarke, G. Archenhold, and N. C. Davidson. A novel technique for determining the 3D spatial distribution of glass fibres in polymer composites. *Composites Science and Technology*, 55:75–91, 1995.
- [17] N. Cristianini and J. Shawe-Taylor. *An Introduction to Support Vector Machines and Other Kernel-based Learning Methods*. Cambridge University Press, Cambridge, 2000.
- [18] P. Dabke, V. Prabhakar, and S. Sheppard. Using features to support finite element idealizations. In *Proceedings of the ASME Conference on Computers in Engineering*, 1994.
- [19] H. Date, S. Kanai, T. Kishinami, and I. Nishigaki. Flexible feature and resolution control of triangular meshes. In *Proceedings of the Sixth IASTED International Conference on Visualization, Imaging, and Image Processing*, 2006.
- [20] N. C. Davidson, A. R. Clarke, and G. Archenhold. Large-area, high-resolution image analysis of composite materials. *J. of Microscopy*, 185:233–242, 1997.
- [21] B. Davis, P. Gramann, and A. Rios. Effect of fiber orientation anisotropies on the structural performance of molded FRP composite parts. Technical report, The Madison Group: Polymer Processing Research Corporation, 2002.
- [22] B. Demir and S. Ertürk. Accurate SVM classification using border training patterns. *First Workshop on Hyperspectral Image and Signal Processing: Evolution on Remote Sensing*, 2009.
- [23] M. B. Dogruoz and M. Arik. An investigation on the conduction and convection heat transfer from advanced heat sinks. In *Proceedings of the 11th Intersociety Conference on Thermal and Thermomechanical Phenomena in Electronic Systems*, pages 367–373, Orlando, FL, 2008.

- [24] R. J. Donaghy, C. G. Armstrong, and M. A. Price. Dimensional reduction of surface models for analysis. *Engineering with Computers*, 16:24–35, 2000.
- [25] C. Eberhardt and A. Clarke. Fibre-orientation measurements in short-glass-fibre composites, Part I: Automated, high-angular-resolution measurement by confocal microscopy. *Composites Science and Technology*, 61:1389–1400, 2001.
- [26] E. Egan and C. H. Amon. Measuring thermal conductivity enhancement of polymer composites: Application to embedded electronics thermal design. *J. of Enhanced Heat Transfer*, 8(2):119–135, 2001.
- [27] S. Egelkraut, C. Heinle, B. Eckardt, P. Kramer, Z. Brocka, M. Marz, H Ryssel, and G. W. Ehrenstein. Highly filled polymers for power passives packaging. In *Proceedings of the 2nd Electronics System Integration Technology Conference*, pages 403–410, London, UK, 2008.
- [28] G. Fischer and P. Eyerer. Measuring spatial orientation of short fibre reinforced thermoplastics by image analysis. *Polymer Composites*, 9:297–304, 1988.
- [29] F. Folgar and C. L. Tucker III. Orientation behavior of fibers in concentrated suspensions. *J. of Reinforced Plastics and Composites*, 3, 1984.
- [30] M. Foskey, M. C. Lin, and D. Manocha. Efficient computation of a simplified medial axis. *J. of Computing and Information Science in Engineering*, 3:274–284, 2003.
- [31] G. Foucault, J. Cuillière, V. François, and J. Léon. Adaptation of CAD model topology for finite element analysis. *Computer-Aided Design*, 40:176–196, 2008.
- [32] J. Y. H. Fuh, Y. F. Zhang, A. Y. C. Nee, and M. W. Fu. *Computer-Aided Injection Mold Design and Manufacture*. Marcel Dekker Inc, 2004.
- [33] L. Gu. A comparison of polynomial based regression models in vehicle safety analysis. *ASME Design Engineering Technical Conf. – Design Automation Conference*, 2001. DETC2001/DAC-21063.
- [34] T. He, L. Hong, A. Kaufman, A. Varshney, and S. Wang. Voxel based object simplification. In *Proceedings of Visualization '95*, 1995.
- [35] D. A. Hemsley, editor. *Applied Polymer Light Microscopy*. Elsevier Applied Science, London, 1989.
- [36] P. J. Hine, R. A. Duckett, N. Davidson, and A. R. Clarke. Modelling of the elastic properties of fibre reinforced composites. I: Orientation measurement. *Composites Science and Technology*, 47, 1993.
- [37] F. P. Incropera and D. P. DeWitt. *Fundamentals of Heat and Mass Transfer*. John Wiley & Sons, Inc., New York, sixth edition, 2007.

- [38] K. Inouea, T. Itoha, A. Yamadaa, T. Furuhatatab, and K. Shimadac. Face clustering of a large-scale CAD model for surface mesh generation. *Computer-Aided Design*, 33:251–261, 2001.
- [39] A. Islam. *Two Component Micro Injection Moulding for Moulded Interconnect Devices*. PhD thesis, Mechanical Engineering, Technical University of Denmark, 2008.
- [40] A. Islam, H. N. Hansen, P. T. Tang, and E. M. Kjær. Bond strength of two-component injection moulded MIDs. In *Proceedings of the 7th International Congress on Moulded Interconnect Devices*, pages 245–254, Fuerth, Germany, 2006.
- [41] N. Joshi and D. Dutta. Feature simplification techniques for freeform surface models. *J. of Computing and Information Science in Engineering*, 3:177–186, 2003.
- [42] E. G. Kim, J. K. Park, and S. H. Jo. A study of fiber orientation during the injection molding of fiber-reinforced polymeric composites (comparison between image processing results and numerical simulation). *J. of Material Processing Technology*, 111:225–232, 2001.
- [43] J. P. C. Kleijnen. *Statistical Tools for Simulation Practitioners*. Marcel Dekker, New York, NY, 1987.
- [44] J. P. C. Kleijnen. Kriging metamodeling in simulation: A review. *European J. of Operational Research*, 192:707–716, 2009.
- [45] J. Y. Lee, J. H. Lee, H. Kim, and H. S. Kim. A cellular topology-based approach to generative progressive solid models from feature-centric models. *Computer-Aided Design*, 36:217–219, 2004.
- [46] K. Y. Lee, C. G. Armstrong, M. A. Price, and J. H. Lamont. A small feature suppression/unsuppression system for preparing B-Rep models for analysis. In *Proceedings of the 2005 ACM symposium on solid and physical modeling*, 2005.
- [47] K. Y. Lee, M. A. Price, C. G. Armstrong, M. Larson, and K. Samuelsson. CAD-to-CAE integration through automated model simplification and adaptive modeling. In *Proceedings of International Conference on Adaptive Modeling and Simulation*, 2003.
- [48] S. H. Lee. A CAD-CAE integration approach using feature-based multi-resolution and multi-abstraction modeling techniques. *Computer-Aided Design*, 37:941–955, 2005.
- [49] S. H. Lee. Feature-based multiresolution modeling of solids. *ACM Transactions on Graphics*, 24:1417–1441, 2005.

- [50] S. H. Lee and K. Lee. Feature-based multiresolution techniques for product design. *J. of Zhejiang University SCIENCE A*, 7:1535–1543, 2006.
- [51] Y. G. Lee and K. Lee. Geometric detail suppression by the fourier transform. *Computer-Aided Design*, 30:667–693, 1998.
- [52] Y. H. Lee, S. W. Lee, J. R. Youn, K. Chung, and T. J. Kang. Characterization of fiber orientation in short fiber reinforced composites with an image processing technique. *Materials Research Innovations*, 6:65–72, 2002. DOI: 10.1007/x10019-002-0180-8.
- [53] P. Luckow, A. Bar-Cohen, P. Rodgers, and J. Cevallos. Energy efficient polymers for gas-liquid heat exchangers. *J. of Energy Resources Technology*, 132(2), 2010. DOI: 10.1115/1.4001568.
- [54] I. G. Maglogiannis. *Emerging Artificial Intelligence Applications in Computer Engineering*. IOS Press, Amsterdam, 2007.
- [55] R. A. Mallow. *Part Design for Injection Molding*. Hanser Gardner Publications, 1994.
- [56] L. T. Manzione, editor. *Applications of Computer Aided Engineering in Injection Moulding*. Hanser, Munich, 1987.
- [57] J. G. Mason, B. W. Farquhar, A. J. Booker, and R. J. Moody. Inlet design using a blend of experimental and computational techniques. In *Proceedings of the 18th Congress of ICAS*, volume 1, 1992. ICAS-92-3.3.1.
- [58] G. Menges, W. Michaeli, and P. Mohren. *How to Make Injection Molds*. Hanser Gardner Publications, third edition, 2001.
- [59] D. Miller, R. E. Holtz, N. Koopman, T. J. Marciniak, and D. R. MacFarlane. Plastic heat exchangers: A state-of-the-art review. *ANL-79-12*, 1979.
- [60] V. Picheny, D. Ginsbourger, O. Roustant, R. T. Haftka, and N. Kim. Adaptive designs of experiments for accurate approximation of a target region. *J. Mechanical Design*, 132:071008, 2010.
- [61] G. Régnier, D. Dray, E. Jourdain, S. Le Roux, and F. M. Schmidt. A simplified method to determine the 3D orientation of an injection molded fiber-filled polymer. *Polymer Engineering and Science*, 2008. DOI: 10.1002/pen.21161.
- [62] K. Robb, O. Wirjadi, and K. Schladitx. Fiber orientation estimation from 3D image data: Practical algorithms, visualization, and interpretation. In *Seventh International Conference on Hybrid Intelligent Systems*, 2007. DOI: 10.1109/HIS.2007.26.
- [63] L. C. Sawyer and D. T. Grubb. *Polymer Microscopy*. Chapman & Hall, London, 1996.

- [64] S. I. S. Shaharuddin, M. S. Salit, and E. S. Zainudin. A review of the effect of moulding parameters on the performance of polymeric composite injection moulding. *Turkish J. of Engineering & Environmental Sciences*, 30:23–34, 2006.
- [65] A. Sheffer. Model simplification for meshing using face clustering. *Computer-Aided Design*, 33:925–934, 2001.
- [66] A. Sheffer, T. Blacker, and M. Bercovier. Clustering: Automated detail suppression using virtual topology. In *ASME 220. Trends in unstructured mesh generation*, Evanston, IL, 1997. ASME.
- [67] T. W. Simpson, J. D. Peplinski, P. N. Koch, and J. K. Allen. Metamodels for computer-based engineering design: Survey and recommendations. *Engineering with Computers*, 17:763–779, 2001.
- [68] A. Sud, M. Foskey, and D. Manocha. Homotopy-preserving medial axis simplification. In *Proceedings of the 2005 ACM Symposium on Solid and Physical Modeling*, 2005.
- [69] T. J. Tautges. Automatic detail reduction for mesh generation applications. In *Proceedings of the 10th International Meshing Roundtable*, 2001.
- [70] A. Thakur, A. Banerjee, and S. K. Gupta. A survey of CAD model simplification techniques for physics-based simplification applications. *Computer-Aided Design*, 4(2):65–80, 2009.
- [71] C. T’Joen, Y. Park, Q. Wang, A. Sommers, X. Han, and A. Jacobi. A review on polymer heat exchangers for HVAC&R applications. *International J. of Refrigeration*, 32(5):763–779, 2009. DOI: 10.1016/j.ijrefrig.2008.11.008.
- [72] C. J. Turner and R. H. Crawford. N-Dimensional nonuniform rational B-splines for metamodeling. *J. of Computing and Information Science in Engineering*, 9:031002, 2009.
- [73] C. J. Turner, R. H. Crawford, and M. I. Campbell. Multidimensional sequential sampling for NURBs-based metamodel development. *Engineering with Computers*, 23:155–174, 2007.
- [74] S. Venkataraman and M. Sohoni. Reconstruction of feature volumes and feature suppression. In *Proceedings of 7th ACM Symposium on Solid Modeling*, 2002.
- [75] G. G. Wang and S. Shan. Review of metamodeling techniques in support of engineering design optimization. *J. Mechanical Design*, 129, 2007. DOI:10.1115/1.2429697.
- [76] S. Yu, X. Yang, Z. Hao, and Y. Liang. An adaptive support vector machine learning algorithm for large classification problem. *Advances in Neural Networks*, 3971:981–990, 2006.

- [77] G. Zak, C. B. Park, and B. Benhabib. Estimation of three-dimensional fibre-orientation distribution in short-fibre composites by a two-section method. *J. of Composite Materials*, 35:316–339, 2001. DOI: 10.1177/002199801772662190.
- [78] H. Zhu and C. J. Menq. B-Rep model simplification by automatic filled/round suppressing for efficient automatic feature recognition. *Computer-Aided Design*, 34:109–123, 2002.